FACULTY OF INFORMATION TECHNOLOGY AND ELECTRICAL ENGINEERING
DEGREE PROGRAMME IN ELECTRONICS AND COMMUNICATIONS ENGINEERING

MASTER'S THESIS

FINE-GRAINED PERFORMANCE ANALYSIS OF MASSIVE MTC NETWORKS WITH SCHEDULING AND DATA AGGREGATION

Author	Nelson Jesús Mayedo Rodríguez
Supervisor	Assist. Prof. Hirley Alves
Second Examiner	Assist. Prof. Onel L. Alcaraz López

February 2021

Mayedo Rodríguez N. (2021) Fine-grained performance analysis of Massive MTC Networks with Scheduling and Data Aggregation. University of Oulu, Degree Programme in Electrical Engineering, 72 p.

ABSTRACT

The Internet of Things (IoT) represents a substantial shift within wireless communication and constitutes a relevant topic of social, economic, and overall technical impact. It refers to resource-constrained devices communicating without or with low human intervention. However, communication among machines imposes several challenges compared to traditional human type communication (HTC). Moreover, as the number of devices increases exponentially, different network management techniques and technologies are needed. Data aggregation is an efficient approach to handle the congestion introduced by a massive number of machine type devices (MTDs). The aggregators not only collect data but also implement scheduling mechanisms to cope with scarce network resources.

This thesis provides an overview of the most common IoT applications and the network technologies to support them. We describe the most important challenges in machine type communication (MTC). We use a stochastic geometry (SG) tool known as the meta distribution (MD) of the signal-to-interference ratio (SIR), which is the distribution of the conditional SIR distribution given the wireless nodes' locations, to provide a fine-grained description of the per-link reliability. Specifically, we analyze the performance of two scheduling methods for data aggregation of MTC: random resource scheduling (RRS) and channel-aware resource scheduling (CRS). The results show the fraction of users in the network that achieves a target reliability, which is an important aspect to consider when designing wireless systems with stringent service requirements. Finally, the impact on the fraction of MTDs that communicate with a target reliability when increasing the aggregators density is investigated.

Keywords: data aggregation, Internet of Things, meta distribution, machine type communication, scheduling schemes, stochastic geometry.

TABLE OF CONTENTS

FOREWORD

This thesis is the result of the research activities conducted at the Center for Wireless Communications (CWC) at the University of Oulu, Finland.

I would like to dedicate this work in first place to God because it is for him that I am still breathing. Thank you Lord for the grace I do not deserve; for lifting me up in my darkest days. Thank you Silvia Rodríguez, "*mi mamita linda*", for being my mother and my best friend as well. Thank you for all your guidance and all the prayers during these years that we have been far from each other. Thank you "*Mima*", for being the best grandmother I could ever ask for. All my achievements will always be dedicated to you.

I would like to express my gratitude to my principal supervisor, Assistant Professor Hirley Alves, for his continuous encouragement and his dedication to transform me not only in a researcher but also in a better human. A spacial space is dedicated to Assistant Professor Onel Luis Alcaraz López for providing me with the correct tools to become a researcher; for his constant support since I arrived to Finland. None of my achievements would have been possible without your valuable advises. Thank you Onel for being part of my family during these years. I am also extremely grateful to Professor Matti Latva-aho, who gave me the opportunity to pursue a master degree in one of the most prestigious places in the world in terms of wireless communications research. Thank you for all the hard work to bring me from the other side of the Atlantic.

I am grateful to all my colleagues from the MTC group for all the great moments we have shared and all the experience I could obtain from each one of you. I will always remember the friendly environment we kept during these years. Some of you still remain in the group and some others have taken different journey but you all have a place saved in my heart.

This thesis was financially supported by Professor Latva-aho's Academy Professor project from Academy of Finland (grant n.307492), 6Genesis Flagship project (grant n.318927), FIREMAN project (grant n.326301) and EE-IoT project (grant n.319008).

Oulu, 11th March, 2021

Nelson Jesús Mayedo Rodríguez

LIST OF ABBREVIATIONS AND SYMBOLS

3GPP	Third-Generation Partnership Project
nG	n-th generation of cellular networks
BS	base station
CH	cluster head
CRS	channel-aware resource scheduling
CSI	channel state information
CDF	cumulative distribution function
D2D	device-to-device communication
DPP	Determinantal point process
eMBB	enhanced mobile broadband
GPP	Gauss-Poisson process
HTC	human type communication
HCN	heterogeneous cellular network
IoT	Internet of Things
IRS	intelligent reflecting surface
LTE	Long Term Evolution
LPWA	low-power wide-area
LoS	line-of-sight
MD	meta distribution
MAC	medium access control
MIMO	multiple-input multiple-output
mMIMO	massive MIMO
MHC	Matérn hard-core process
MCP	Matérn cluster process
MTC	machine type communication
MANET	mobile ad-hoc network
mMTC	massive MTC
mm-Wave	millimeter wave
M2M	machine-to-machine
NOMA	non-orthogonal multiple access
MTD	machine type device
PPP	Poisson point process
PP	point process
PGFL	probability generating functional
PHP	Poisson hole process
PDF	probability density function
QoS	quality of service
RF	radio frequency
SIR	signal-to-interference ratio
SNR	signal-to-noise ratio
SINR	signal-to-interference-plus-noise ratio
SG	stochastic geometry
SIC	successive interference cancellation
UDN	ultra dense network
UAV	unmanned aerial vehicle

URLLC	ultra-reliable low-latency communication
VANET	vehicular ad-hoc network
V2V	vehicle-to-vehicle communication

Symbols:

θ	SIR threshold
α	path loss exponent
λ	density of a PP
L	local delay
x	target reliability
$p_s(\theta)$, p_s	standard success probability. Both representations are used indistinctly
$P_s(\theta)$	conditional success probability
K	instantaneous number of MTDs requesting service
m	average number of MTDs around each aggregator
N	number of orthogonal channels available at each aggregator
R_D	clusters' radius
Φ_p	aggregators PP
Φ_I	interference PP
λ_p	intensity of Φ_p
λ_I	intensity of Φ_I
h	channel power gain corresponding to direct links
g	channel power gain corresponding to interfering links
P_0	average channel occupation probability
Λ	intensity measure (or first-order moment measure)
$G(r)$	nearest-neighbor distance distribution function
$g(r)$	pair correlation function
$\mathcal{K}(r)$	Ripley's function
$F(r)$	contact distribution function
$\bar{F}(\cdot)$	MD of the conditional success probability
M_b	b-th moment of the conditional success probability
G_0	deployment gain
$\tilde{\theta}$	random SIR threshold
R_D	clusters' radius where the MTDs are located around the aggregators
r_d	uniform distributed distance of MTDs from the aggregators
Ψ	MTDs PP (MCP)
$\mathcal{N}$	set of orthogonal channels available at the aggregators
y_i	distance from the i-th MTD interferer to the typical point
ρ	full inversion power control constant

Mathematical operators:

$\triangleq$	definition
$\mathbb{Z}^+$	set of positive integer numbers
$\mathbb{R}$	set of real numbers
$\mathbb{N}$	set of natural numbers
$\mathbb{R}^d$	d-dimensional Euclidean space

$\Im(\cdot)$	imaginary part
$\Re(\cdot)$	real part
j	imaginary unit, e.g. $\sqrt{-1}$
$\exp(z)$, e^z	exponential function of z. Both representations are used indistinctly
$\mathrm{Var}(\cdot)$	variance operator
$\mathbb{E}(\cdot)$	expectation operator
$\mathbb{E}^{!0}(\cdot)$	expectation with respect to the conditional probabilities
$I(a,b)$	regularized incomplete beta function
$B(a,b)$	beta function
$f_Z(z)$	PDF of continuous random variable Z
$F_Z(z)$	CDF of the random variable Z
$\Gamma(\cdot)$	gamma function
$\Gamma(\cdot,\cdot)$	upper incomplete gamma function
$\mathcal{B}(z,r)$	d-dimensional (closed) ball of radius r centered at z
$\lvert\cdot\rvert$	cardinality in case of a set, absolute value, and the Lebesgue measure (for example, in two dimensions, the area of a disk of radius 2 is $\lvert b(o,2)\rvert = 4\pi$)
$\lvert\lvert\cdot\rvert\rvert$	2-dimensional Euclidian norm
$\lfloor z \rfloor$	largest integer smaller than or equal to z
$\binom{\cdot}{\cdot}$	binomial coefficient
$\mathbb{1}(\cdot)$	indicator function
$\equiv$	equivalence in distribution
$(\cdot)$	minimum operator
$\ln(\cdot)$	natural logarithm
$\mathbb{P}(A)$	probability of event A's occurrence
$\mathcal{L}_Z(s)$	Laplace transform of the random variable Z

Distributions:

Poiss(m)	Poisson distribution with mean 'm' such that $P_Z(z) = \frac{m^z e^{-m}}{z!}$
Levy(μ, ϑ)	Lévy distribution with location parameter μ and scale parameter ϑ
Exp(m)	exponential distribution with mean 'm' such that $f_Z(z) = \frac{1}{m} e^{-\frac{z}{m}}$, $z > 0$

1 INTRODUCTION

During the last decades, the world witnessed notable advances in wireless technologies in terms of human communication. Evolving from only voice services offered by the first generation (1G) cellular networks; stepping forward to the starting phase of the second generation (2G) with features and services such as signal digitalization, short text messages and email transfers but at 14.4 kbps data rates; following with the third generation (3G) providing digital broadband and enhanced downlink data transmission speed ranging from 8 Mbps to 10 Mbps; to finally reach 100 Mbps and broader coverage using forth generation (4G) technology [1]. This evolution allowed cellular networks to move progressively from voice-centric to data-centric systems, but still, communication was restricted to humans.

Recently, a growing interest arose from academia and industry to provide worldwide connectivity among *things* (machines and devices). This transition from human type communications (HTC) toward machine type communications (MTC) is driven by the need to reform our society and, therefore, the way we live. Moreover, even though the technology to connect *things* to the Internet has existed for more than 20 years, the actual development in embedded devices, smart user interfaces, and cloud computing[1] impulses the Internet of Things (IoT) concept to emerge as a huge potential value in terms of improved efficiency, sustainability and safety for industry and society [3]. Under this huge umbrella, the recently introduced fifth generation (5G) New Radio is designed to moderately support massive and critical MTC. However, it is clear that 5G cannot support the new and stringent requirements on wireless connectivity that most novel and futuristic MTC applications may impose [4]. In this context, sixth generation (6G) is envisioned to incorporate suitable technologies defined outside the 5G scope, that will change the way wireless networks collect, process and transmit data [5].

1.1 IoT applications and challenges

Recently, IoT-based services have gained enormous popularity, and are expected to keep growing in the future. Some of the most important IoT applications to improve human life and contribute to the world's economic growth include:

- smart home, often referred to as home automation, enables the remote monitoring and management of appliances and systems, such as lighting and heating [6];
- wearables or smart electronic devices located close to the skin's surface to detect, analyze, and transmit information related to body signals and/or data collected from the environment. This allows, in some cases, immediate feedback to the person wearing it [7];
- smart grids [8], which is the traditional electrical network serving every citizen, but updated with communication technologies such as sensors, radio modules, and gateways. This technology allows consumers to make better energy usage

[1]Device computation can be offloaded to the cloud to benefit from on-demand self-service, resource pooling, broad network, measured service, and rapid elasticity [2]

decisions to save electricity and reduce the expenses associated with high energy consumption, and permits to restore power faster after a collapse;

- connected vehicles, see [9], is another application that might help in preventing accident by optimizing driving decision making, and avoiding long traffic queues (improves traffic flow) due to the constant interchange of information related to location, speed, and dynamics among vehicles and road infrastructure such as traffic lights;

- smart farming [10], which involves data collection from sensors and monitoring to elaborate analytical models that farmers can use to make more accurate decisions about crops harvesting and rearing.

Figure 1 shows some IoT applications and the ecosystem of network technologies to support the variety of requirements. The requirement differences (latency and data rate)

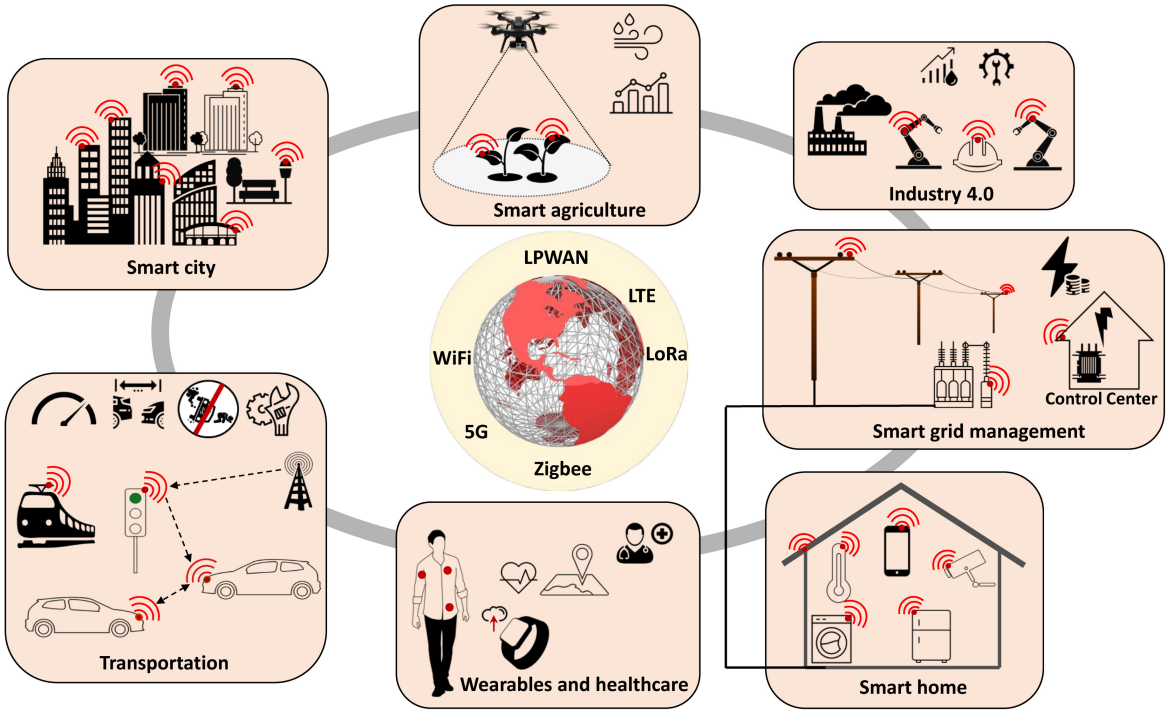

Figure 1. Internet of Things ecosystem.

between some of these application domains are described in [11]. These applications bring brand-new business opportunities while imposing numerous challenges in connectivity and efficient communication management.

Because most IoT devices are placed in remote areas, depending on the application, they use wireless connectivity; therefore, the existing wireless infrastructure demands substantial changes. Widely adopted wireless communication protocols such as orthogonal frequency-division multiplexing require additional circuitry; thus, they need to be redesigned to fit IoT scenarios [12], [13]. Moreover, short-range wireless technologies (communication over centimeters) are essential to ensure the desired low-complexity IoT devices and the required low-cost deployments.

IoT devices mainly include four stages to complete a particular task: data acquisition;

data processing, which is the most time-consuming; data storage and data transmission and communication, which is the one that consumes more power. Thus, it is critical to consider energy-efficient designs in all these stages [14]. In this sense, energy harvesting technologies [15, 16], low-power processors units [17, 18], and efficient duty cycling[2] techniques [19] can contribute to avoid traditional large and heavy batteries and power packs, which are not suitable for small IoT devices.

In general, most IoT devices are deployed to sense the surrounding environment, generate raw data and transmit this information to other nodes in the network. In industrial scenarios, this real-time data is exploited to make better decisions, improve productivity and save human's life, e.g., manufacturing industry [20] and safer mining industry [21]. However, extracting useful information from a highly dynamic environment and perform actions based on it (e.g., detecting anomalies and correct them) is a challenging research problem in artificial intelligence [22], [23]. Particularly, machine learning-based approaches allow users to identify patterns in historical data to visualize tendencies that appear over long periods and run predictive analysis based on a variety of possible scenarios. However, implementing complex machine learning algorithms in resource-constrained devices to achieve these goals is a big challenge [24]. This is because the algorithms need match the storage capacity and computing power of IoT devices.

On the other hand, machines and objects in practically any industry scenario can be connected and configured to send data to cloud applications over diverse network technologies working in licensed and unlicensed bands [25], [26]. Thus, a security risk is present at every link along the IoT path. Unfortunately, diverse kinds of traffic, devices' computing capabilities, and the lack of a common standard and architecture for IoT protection make security solutions a tough assignment [27], [28].

1.2 5G-enabled IoT

Cellular technologies can provide clear benefits across a wide range of IoT applications. This is mainly because: *i*) reduced deployment costs by re-using the already existing infrastructure with global reach, *ii*) high scalability, *iii*) mature quality of service (QoS) functionalities and *iv*) security [29]. However, current cellular networks such as Long-Term Evolution (LTE), conceived for mobile broadband traffic with target block error rate of 10^{-1} and unpredictable latency values that ascend to several seconds [30], cannot efficiently support connectivity for a massive number of heterogeneous devices[3] communicating between each other through the Internet with low or without human supervision.

5G networks address previous standard limitations by introducing a set of enabling technologies that provide energy and spectral efficient connectivity. This includes device-to-device (D2D) communications, massive multiple-input multiple-output (mMIMO), communications in the millimeter wave (mm-Wave) spectrum, and ultra dense networks (UDN).

[2]An IoT device spends most of its time in the sleep mode; thus, it is essential to find promising solutions for very large-scale integration (VLSI) designs that reduce the static power consumption (leakage) [14].

[3]The number of IoT devices, e.g., sensors, actuators, appliances, is foreseen to reach 38.6 billions by 2025 [31].

D2D communication refers to a radio technology that enables user equipments located in close proximity to bypass the cellular base stations (BSs) and directly connect to each other, which is extremely beneficial for users located at the cell edge or congested areas. Notice that other short-range technologies such as Bluetooth, WiFi or near-field communication provide some D2D communication functionalities. However, they work in unlicensed band; thus, the interference is unmanageable and they cannot provide security and QoS guarantees as cellular networks do [32]. D2D communication is a promising solution to improve spatial frequency reuse, decrease the power consumption in cellular networks, reduce the traffic congestion at the network core and minimize the latency. However, its implementation involves technical challenges such as interference management, peer discovery, synchronization, resource allocation for D2D and cellular links, and adaptive mode selection and power control for user equipments [33]. The most popular use cases of D2D communication include public safety services, mobile tracking and positioning, traffic offloading, vehicle-to-vehicle (V2V) communication, content distribution, extension of cellular coverage and reliable health monitoring [34].

mMIMO is a fundamental technology for providing the high spectral efficiency[4], energy efficiency and reliability professed by 5G. This concept emerged in 2010 and it was considered science fiction at that time [36] but it became a commercial reality in 2018 [37]. In general, large-scale antenna arrays permit to concentrate all the power in specific directions by implementing very sophisticated algorithms such as beamforming (precoding) and beam steering [38]. Moreover, since mMIMO uses many more antennas (typically more than 64) than the number of users served in a resource block, the beam can be extremely narrow, thus reducing the leakage in undesired directions; which translates to high-efficient signal energy transmissions and very limited (if any) interference. Also, notice that narrow signal beams, which implies high angular resolution, make the user position tracking process more reliable. Although mMIMO adds undeniable qualitative improvements over conventional MIMO, researchers still need to address some challenges such as pilot contamination, precoding, channel estimation, user scheduling, and hardware impairments [39]. Authors in [35] discuss important considerations for mMIMO design, optimization and deployment.

mm-Waves communications operate over a high frequency spectrum (from 30 to 300 GHz) and bring attractive opportunities to attain ultra-high data rates by exploiting large signal bandwidths. Moreover, using higher spectrum frequencies allows to reduce the dimensions of an antenna and pack more antennas into an array; this is why mm-Waves is the primary enabler of mMIMO. The key research challenges come from the inherent propagation characteristics of electromagnetic waves at high frequencies. mm-Wave transmissions experience high attenuation because of their incapacity to penetrate objects (rich scattering concept completely disappears) and their molecular-specific absorption loss. The path loss effects on the received power at high frequencies can be drawn from Friis transmission equation [40], and can be compensated by using antennas with high gains or equivalently exploiting the high

[4]Spectral efficiency is the number of information bits per complex-valued sample, measured in bit/s/Hz, that it can be transmitted reliably over the specific channel [35]. It refers to the capability of using the bandwidth efficiently.

gain from large antenna arrays. Moreover, since the *coherence block*[5] is proportional to the wavelength, estimating the time-varying channel in mm-Wave bands requires more updates, which results in greater pilot overhead than in sub-6 GHz band [41], [42]. Also, notice that at mm-Wave frequencies, the noise power, which is proportional to the bandwidth, cannot be neglected; thus, effective beamforming for pilots is crucial to improve the signal-to-noise ratio (SNR). Due to the aforementioned issues, it is expected that mm-Wave technologies can be efficient only in the context of short-range communication; furthermore, it is essential to develop accurate channel and propagation models that account for parameters such as line-of-sight (LoS) probability, large-scale path loss and building penetration loss to exploit their full benefits.

The main idea behind UDN is to move the access nodes as close as possible to the end users by deploying low-power small cells (picocells and femtocells) in the coverage area of traditional macrocells, particularly, in hotspots where high traffic is generated [43]. The density of cells is greater than that of active users [44]. This allows to satisfy the stringent and diverse users' requirements while providing uniform coverage and adaptable connectivity. In this context, the integration of unmanned aerial vehicles (UAVs) as small cells for temporarily restoring service is studied in [45]. This is beneficial due to the strong LoS links that UAVs can provide and the possibility of rapid and low-cost deployments. However, UDNs introduce new technical challenges such as load imbalance, severe interference problems, unfairness in radio resource sharing, unnecessary handover, inefficient radio resource utilization and high signalling overhead. Moreover, recent studies reveal that at certain point, network densification may stop providing significant throughput gains. In other words, the coverage probability in terms of the signal-to-interference-plus-noise ratio (SINR) is maximized at a finite BS density beyond which the throughput decreases [46]. For instance, authors in [47] show that the coverage reaches a maximum point before starting to decay when the network becomes denser under bounded pathloss, lognormal shadowing and strongest cell association. Physical limitations in the UDNs performance such as the BS height is studied in [46]. To overcome these challenges and achieve the performance requirements in 5G, it is essential to combine UDNs and other 5G enabling technologies such as mMIMO and mm-Wave [48].

Notice that 5G does not only presuppose high data rates transmissions, as it is commonly thought; but it is a whole ecosystem of technologies that will support a wide range of use cases and requirements. In particular, the Third-Generation Partnership Project (3GPP) considers enhanced mobile broadband (eMBB), ultra-reliable low-latency communications (URLLC), and massive MTC (mMTC) as three main use cases that 5G should support. Important design criteria for each 5G service are discussed in [49], while authors in [50] investigate the heterogeneity arising from their coexistence, under orthogonal and non-orthogonal slicing of radio resources. Notice that efficient resource sharing between mMTC and URLLC users is challenging to accomplish due to the random activity of users belonging to the first group, and deserve special attention since they constitute enablers for a broad spectrum of IoT applications.

In one extreme case, URLLC is introduced to support use cases with stringent

[5]A *coherence block* consists of several subcarriers and time samples over which the channel response remains constant. If the coherence bandwidth is B_c and the coherence time is T_c, then each coherence block contains $\tau_c = B_c T_c$ complex-valued samples [35].

requirements in terms of extremely low latency[6](less than 1 ms), high availability and reliability[7] (say 10^{-9} of decoding error probability). Specifically, it is expected to play an important role in providing connectivity for new scenarios from vertical domain (critical IoT) [54] such as factory automation, with a maximum error probability of 10^{-9} and latency ranging from 0.25 to 10 ms; smart grids (10^{-6} and $3-20$ ms, depending on each country electricity frequency); intelligent transportation (10^{-5}, $5-10$ ms) [30], etc. Notice that when the latency requirement is not a most, transmitting at a rate lower than channel capacity guarantees the target reliability almost surely, but ensuring low latency and high reliability in parallel makes URLLC extremely challenging [55]. On the other extreme, mMTC networks are designed to be latency-tolerant, and the main performance requirement is to provide connectivity for a huge number of devices that sporadically transmit and receive a small amount of data [56]. Since these devices are battery-powered, the major concern lies in changing the traditional protocol stack and network structure to utilize the available power sparingly.

This thesis focuses on mMTC; thus, in the next section, we present the challenges and requirements on massive connectivity. Moreover, we introduce the main mMTC characteristics that impose a redesign of traditional HTC protocols.

1.3 Challenges and requirements for massive connectivity

In contrast to HTC, mMTC brings new network designs and associated challenges to be addressed. For example, HTC is characterized by high-speed downlink communication, while low-rate uplink transmissions (data rate for each user may be around 10 kbits/s [57]) prevail in mMTC. Since the payload size can be similar to that of the data packets[8], novel techniques for short packet length transmission need to be studied to prevent the overhead resulting from the control signals (messages required before the data payload is transmitted successfully) such as new channel coding mechanisms [58], low signaling overhead medium access control (MAC) protocols [59] and grant-free communication with appropriate collision resolution mechanisms [60]. Notice that less frequent and shorter transmissions preserve energy; thus, low signaling overhead MAC protocols also constitute an enabler for energy efficient MTC. As the number of devices increases exponentially, e.g., up to 300.000 devices in a single cell [57], the radio spectrum becomes insufficient to support the variety of applications; thus, non-orthogonal multiple access (NOMA) [61] techniques emerge as a prospective solution to allow signal overlapping over the same time-frequency resources via power-domain or code-domain multiplexing. At the receiver side, devices use successive interference cancellation (SIC) when decoding. Notice that orthogonal medium access statically links the number of available resources to the number of tolerable users, which is

[6]Latency is a cross-layer concept. This is, it can be interpreted in many ways according to the focused layer of the communication protocols [51]. For instance, authors in [52] define it as the delay that a data packet experiences from the access of a given protocol layer at the transmitter to the egress of the same layer at the receiver.

[7]Spatial diversity —switching-like combining schemes—is a promising technique to endure the desired reliability levels in URLLC for low-cost IoT devices [53].

[8]Vehicle-to-Everything communication is a typical example that involves the transmission of short information payloads.

inefficient in dense networks. Due to the group-based nature of communication [62], mMTC traffic usually presents high temporal and spatial correlation properties. In other words, the interference, which depends on the active nodes set and is a main limiting factor of wireless network performance, is temporally and spatially correlated. The temporal correlation affects retransmission strategies, while the spatial correlation influences the routing part [63]. Learning techniques are usually needed to extract the correlation information. The data traffic produced by machine type devices (MTDs) is highly heterogeneous, sporadic due to uncoordinated sleeping cycles, and dynamic with event-driven and periodic activations compared to more predictable HTC traffic [57]. For example, in a wireless sensor network, each sensor measures different variables e.g., temperature, humidity, speed, etc, with different characteristics such as dynamic range and frequency. This imposes a variety of hardware restrictions such as sample rate, resolution and sensitivity. Network slicing of wireless resources is a novel solution that can enable HTC and mMTC co-existence in the future cellular networks [64].

Different MTC applications have distinct characteristics and service requirements, e.g., in terms of priority and delay constraints, which leads to the need for novel scheduling schemes. Moreover, MTDs should be cheap enough to allow for massive deployments. This is translated into low complexity, computational and memory resource constraints, and, unfortunately, limited performance. Furthermore, because IoT devices can be placed in locations of hard accessibility and due to the cost associated with battery replacement, power-saving methods for dense IoT networks need to be considered[9]. Low-power wide-area (LPWA) technologies such as LoRa and Sigfox are among the potential technologies to provide cost-effective and long-range (15 km and 20 km, respectively) connectivity solutions for IoT applications [66]. Notice also that energy-efficient clustering schemes simplify the deployment of low-power MTDs [67].

1.4 Reaching beyond 5G

Although 5G aims at supporting several IoT services, it might fall short to meet all novel application requirements. MTC networks in beyond 5G and 6G are envisioned to optimize the integration of a diverse set of communications systems and technologies such as cell-free mMIMO (distributed MIMO), which consists of a group of antennas spread over a large geographical area in such a way that each user is surrounded by BS antennas instead of each BS being surrounded by users as current scenarios showcase. Conventional MIMO BSs with packed arrays cover many users within the corresponding cells, and the received signal strength between different users experiences large variations. Contrary, in cell-free mMIMO, the cell concept disappears and service antennas coherently serve all user terminals; thus, providing higher throughput [37]. The antenna elements may connect each other inside a single cable, e.g., the so-called radio stripes [68], to provide coverage in places where BSs are challenging to deploy, e.g., cultural places, stadiums and factories. A central baseband processing unit is connected to all the antenna stripes to perform the necessary baseband signal processing.

Similar to mMIMO, intelligent reflecting surfaces (IRS) [69], or reconfigurable

[9]The battery of these devices is expected to last more than 10 years with the battery capacity of 5 Wh [65].

intelligent surface [70] could be a keystone to reduce energy consumption in 6G at communication frequencies above 100 GHz while realizing high beamforming gains. IRSs form large and thin metamaterial surfaces that modify the incident electromagnetic waves' phase and amplitude. Thus, producing scatterings in desired directions and reducing the power loss generated by random reflections, which creates an alternative transmission path when the line-of-sight between the transmitter and receiver is obstructed. Note that mMIMO uses beamforming to also secure physical layer communications. However, the achievable secrecy rate is limited even with this technique when the legitimate user and the eavesdropper links exhibit high correlation. In this scenario, IRS can constructively direct the beamformed signal towards the user and in a destructive manner towards the eavesdropper. However, this approach requires detecting and locating the eavesdropper, which is not an easy task. IRSs also make the wireless channel highly controllable, which reduces transmitter and receiver design complexity, and can be utilized in full-duplex relaying applications [71]. This technology will be essential for high-frequency communications where the penetration loss is significant. Moreover, IRSs do not require radio frequency (RF) components; thus, large structures can be potentially produced at low cost and complexity, which translates to less power depletion than conventional active MIMO arrays [71].

Despite the efforts to efficiently exploit mm-Wave spectrum for 5G wireless networks, the quest for increasing data rates persists. The THz band (0.1-10 THz) offers much higher transmission bandwidths than the mm-Wave; however, to achieve its full potentials, several challenges still remain. For instance, THz transmissions experience even higher propagation losses, thus, limiting the communication distances, although suitable beamforming may overcome this issue [72]. Moreover, before the actual data transmissions take place, user equipments communicating at THz frequencies must follow a beam training process to allows transceivers direct the antenna gain toward different directions to find the optimal spatial path that maximizes the received signal. This is not a trivial task to accomplish since it must be repeated to maintain high data rates across the network when the users move and the environment changes [73]. At these frequencies, parasitic reactances of active devices such as transistors increase, which make power amplifiers difficult to fabricate [74]. Even though we can find in the literature several attempts to minimize the receiver complexity by using simpler Schottky barrier diode-based envelope detector to reconstruct the signal coherently [75], THz receivers are still complex and expensive. Moreover, it is necessary to design fast processing chips to handle the wide bandwidth and very large-scale antenna, which consume high power since dynamic power consumption of a chip is proportional to the operating frequency [76].

Figure 2 illustrates a typical UDN with other enable technologies such as mMIMO, mm-Wave, D2D communication and IRS.

1.5 Thesis contributions

Motivated by the crucial role of mMTC in IoT and the challenges arising from the variety of new IoT applications, we devote this thesis to analyze data aggregation and resource scheduling as two crucial techniques to deal with the massive access of MTDs while guaranteeing the desired QoS in these challenging scenarios. We use the novel

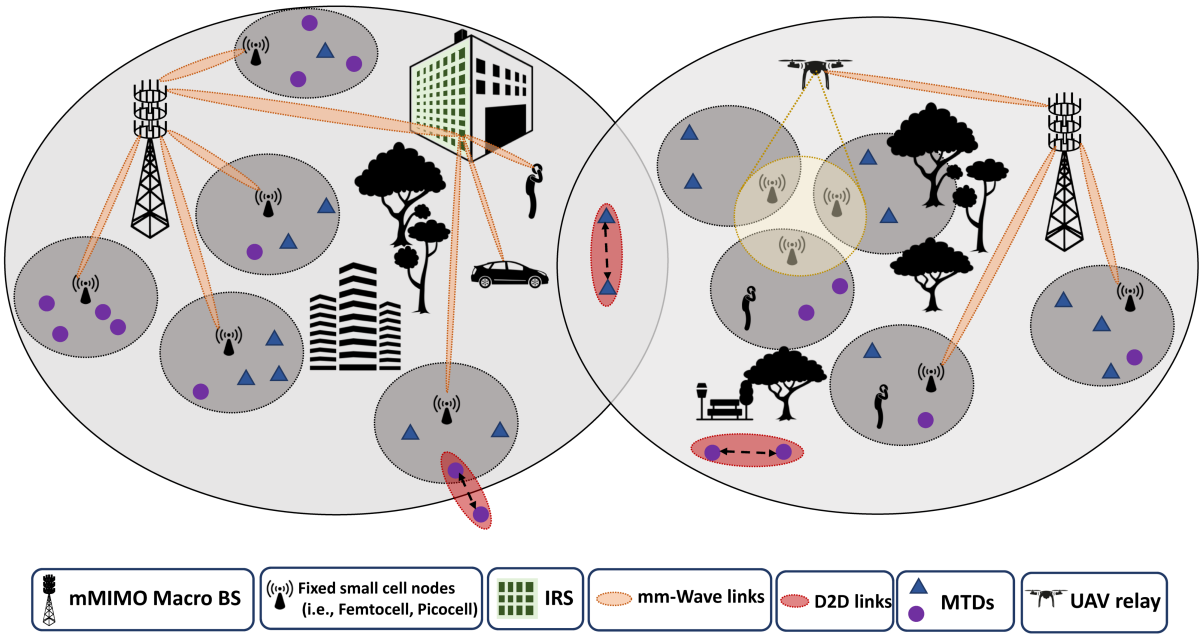

Figure 2. 5G and 6G technologies to support IoT.

concept of meta distribution (MD), a powerful stochastic geometry (SG) tool to handle the per-node QoS requirements. We derive theoretical results, discuss them, and conduct performance evaluation via Monte Carlo simulations in MATLAB. To the best of our knowledge, current literature lacks a framework that integrates the three aforementioned concepts: data aggregation, MD, and resource scheduling. Thus, by integrating them, we provide benchmark performance and important insights to consider in the design of future networks with stringent service requirements. Our objective is to fill this gap through the following concrete contributions:

- We present an overview of the most important SG aspects to model dense networks, e.g., the most common point processes (PPs) used in the literature. Essential metrics to characterized the goodness-of-fit when approximating real network deployments by PPs are also provided.

- We use the MD concept to fully characterize the uplink traffic performance in a Poisson network with data aggregation. We adopt the random resource scheduling (RRS) and channel-aware resource scheduling (CRS) scheduling schemes proposed in [77] to deal with the limited spectrum resources. However, herein we provide a more fine-grained performance characterization of a typical link.

- We present an accurate and simple closed-form expression for the MD of the signal-to-interference ratio (SIR) under the RRS scheme based on an approximation obtained from the relation between the geometric and the arithmetic mean, in contrast to the usually adopted moment inversion approach (Gil-Pelaez theorem) that requires the calculation of complex integrals.

- We also provide an upper bound to the MD under RRS for any path loss exponent ($\alpha \geq 2$) that allows fast computation compared to time-consuming Monte Carlo simulations, and obtaining important network performance insights.

- Our results show that CRS can serve more devices than RRS for a common target reliability. Moreover, we conclude that the standard success probability does not guarantee QoS for any node in a network. We also provide insights into the transmission rate required to keep a percentage of devices/users communicating with a target reliability for both scheduling schemes.

Finally, the exhaustive bibliography review carried out in this thesis can serve as a reference material for master students and researchers working with SG tools to analyze dense wireless networks.

1.6 Thesis outline

The rest of the thesis is organized as follows: Chapter 2 reviews data aggregation, scheduling and resource allocation techniques, and the SIR MD as a powerful SG tool for mMTC with QoS guarantees. Chapter 3 introduces the system model, a MD-based analytical approach for mMTC, and presents the network performance evaluation and numerical results under RRS and CRS. Finally, Chapter 4 concludes the thesis and also discusses future research directions.

2 MASSIVE MTC WITH QOS GUARANTEES

Recently, enabling massive access with QoS guarantees has been of great interest to academia and industry research community. The most common techniques discussed in the literature to handle random access in MTC scenarios are classified as: *i*) direct orthogonal access, *ii*) direct non-orthogonal access, and *iii*) indirect access. The first one includes techniques such as Access Class Barring [78], distributed queuing [79], and dynamic allocation of the random access channel. These solutions aim to reduce preamble collisions' effects; however, the access delay and the signal overhead increase in dense networks. In contrast, non-orthogonal multiple access schemes allow resource overloading, thus fitting to scenarios with a large number of MTDs but sacrificing complexity at the decoder side. The third class refers to cluster-based data aggregetaion, which is treated in detail in the next section.

2.1 Data aggregation

A promising way to support a massive number of concurrent connections emerges from the concept of data aggregation. Moreover, because power-constrained MTDs may not communicate directly with the BS, hierarchical architectures may be necessary to provide efficient data aggregation. This means that MTDs can form groups or clusters, statically or dynamically, depending on some criteria such as QoS, device type, geographic location, services type, and cooperative grouping [80]; and associate to more powerful nodes (in terms of storage and processing capacity) called gateways or aggregators. In general, the density of aggregators is considerably smaller than the density of MTDs. This approach allows aggregators to first collect the data traffic from MTDs and then relay it to the core network, where it is used by multiple applications. As shown in Figure 3, this hierarchical structure [81]: *i*) shortens the distance in the communication while diminishing the power consumption of the MTDs; *ii*) reduces the number of connections to the core, thus decreasing the congestion; and *iii*) extends network coverage. Notice that in the sensor networks context, data aggregation benefits from the intrinsic spatial-temporal correlation that arises from local sensor clustering to remove redundant information.

Dynamic centralized clustering algorithms rely on a sink or BS to select the cluster heads (CHs). To do so, the BS requires extensive data from the nodes, which sometimes needs complex embedded hardware or exchanging a significant number of control messages. In contrast, the nodes in distributed clustering algorithms are completely autonomous since they decide the suitable CHs by exchanging information with each other. Both centralized and distributed clustering algorithms usually alternate the nodes playing the role of the CHs, based on the remaining CH energy, to dynamically balance the energy consumption and the traffic among all the nodes and extend network lifetime [82]. For instance, a distributed approach for data aggregation, where nodes use a fuzzy-logic system to decide whether they become a CH or not, is proposed in [83]. This process is occasionally supported by the BS, which sends three messages during the network lifetime to reconfigure the network's *skip* value, i.e, number of rounds in which the same CHs remains. Authors in [84] propose a centralized clustering mechanism where BS determines the CHs based on location and mobility information received from the MTDs, and runs the k-means algorithm to form the clusters based on how frequent MTDs access

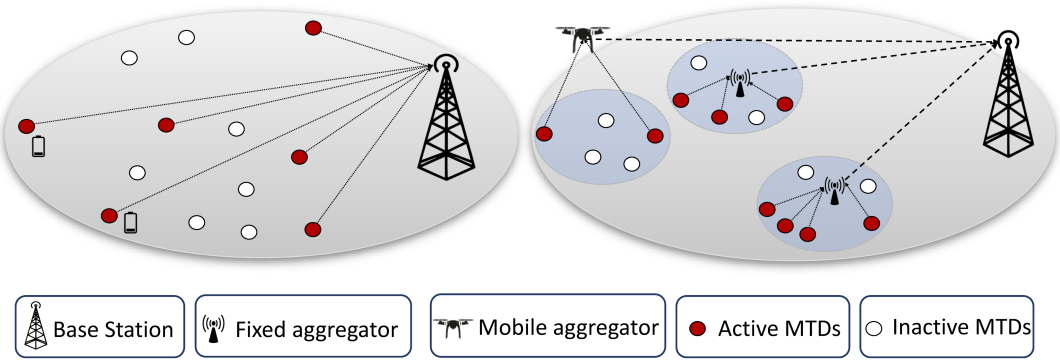

Figure 3. Direct communication between MTDs and BS (left) and a typical data aggregation scenario using fixed data aggregators and a UAV as mobile aggregator (right).

the network. More complex scenarios implement static and dynamic clustering-based data aggregation techniques simultaneously in the network [85]. This approach exploits the assumption that dynamic clustering is more favorable for sensed targets located far from the sink, and events sensed near the sink can be directly transmitted without any aggregation at all. In practice, dynamic clustering mechanisms need to evolve to reduce the signaling overhead and delay associated with cluster formation, e.g, cost from discovering all potential MTC-aggregator links, especially for time-sensitive industrial applications with stringent delay constraints. For example, authors in [86] propose an algorithm to form clusters and select the CHs in vehicular ad-hoc networks (VANETs) based on the regular transmission of beacons to distribute the nodes' states. Excessive beacons transmission results in severe performance degradation due to uncontrolled collisions, especially in high-mobility and dense scenarios. Cluster-based data aggregation mechanisms can improve efficiency if green technologies such as energy harvesting are also implemented. Note that due to the low power budget of MTDs, it is reasonable to let them collect energy from the RF signal sent by aggregators, which in turn, have greater capabilities.

Since MTDs are power and range-limited, data aggregation can appear over multi-hop D2D connections. This is the case of tree-based data aggregation [87, 88] that aims to minimise resource consumption and maximise data collection rate. Data information flows from leaf nodes to the root node or the sink. However, optimizing the hierarchical organization of devices and energy-efficient data aggregation simultaneously dictates critical design issues. This is because the number of hierarchical levels determines the number of transmission hops and therefore the power consumption during the aggregation process. Notice that the number of hops also affects the communication delay, which is extremely linked to the network throughput. Moreover, each time an application traffic changes or a new application emerges, the structure needs to be optimized again based on the new requirement. Even more, in case of packet loss at any stage of the tree, the entire information is affected as well [89].

Recently, several works have taken steps forward by investigating and exploiting the advantages of data aggregation. For instance, authors in [90] propose an energy-efficient data aggregation scheme for a three-stages hierarchical MTC network. Stages composed of transmitters and aggregators can work in parallel or series. In the former, transmission

and aggregation occur simultaneously during all multi-hop transmission stages; although causing severe interference problems. In contrast, the latter does not allow stages to repeat before the data is eventually transmitted to the BS (complete cycle); thus, provides low data rates but causes low interference since multiple stages are not active simultaneously.

Data aggregation benefits can be materialized by deploying either fixed or mobile data aggregators as illustrated in Figure 3. The former constitutes a smart strategy to collect, process, and transmit compressed data in MTC scenarios with low-mobility or static devices such as smart utility meters or video surveillance cameras. This implies knowing the devices' locations to implement suitable aggregation algorithms. A strategically fixed positioned data aggregator can successfully meet the QoS requirements of all MTDs in its vicinity. However, its sub-optimal placement may result in inefficient energy consumption due to variable distances from MTDs to the aggregator. Moreover, massive transmission requests may overload a limited-resource and fixed data aggregator. Deploying mobile data aggregators can solve these issues; however, this solution may be inappropriate for delay intolerant MTDs [91]. Interesting scenarios include UAVs playing the role of mobile aggregators [92], which provide more scalability since UAVs can access outlying areas.

Instead of conventional aggregation schemes based on device location, authors in [93] consider the latency requirement as an essential classifier for MTC services and the fundamental metric to achieve QoS-based aggregation for network slicing. Once the clusters are formed using the k-means algorithm, they are assigned to specific gateways through the Hungarian algorithm. Meanwhile, authors in [91] propose a cooperative data aggregation scheme based on the coexistence of a fixed data aggregator and multiple mobile data aggregators selected using graph theory to aggregate data from delay intolerant and tolerant MTDs, respectively. Notice that it is unlikely that all the MTDs in an mMTC network demand uniform QoS services; thus, this approach provides effective congestion control and energy efficiency while coping with the sub-optimal positioning issues. It also improves the communication delay and outage probability compared to schemes based on single fixed data aggregator and single mobile data aggregators.

Notice that data aggregation is a more complex network functionality that include other aspects such as efficient routing protocols and suitable data aggregation functions to remove the redundant information. Moreover, the trade-off among performance measures such as energy consumption, latency and data accuracy is indispensable to design proper data aggregation structures and protocols. However, in this thesis, we only exploit the cluster-based spatial hierarchy to analyze other network capabilities such as resource scheduling.

2.2 Scheduling and resource allocation

Due to the massive access requests in MTC applications, spectrum scarcity remains a serious issue. Note that communication at higher frequencies (THz and mm-Waves) for mMTC applications imposes a huge challenge since they involve resource constrained-devices located in remote places facing severe propagation problems, e.g., underground locations. Thus, different techniques have been proposed to efficiently manage the insufficient resources. Spectrum sharing is a promising strategy to address the disparity between limited spectrum resource and traffic demands by allowing more than one node

to use the same spectrum at the same time [94]. Among them, cognitive radio based solutions allow MTDs to sense the spectrum and opportunistically access the unused bands in their vicinity without affecting the spectrum utilized by primary users, although this may be costly in terms of device complexity and battery depletion [95], [96]. While mMTC applications can exploit both unlicensed and licensed bands, the former becomes highly problematic due to uncontrolled interference (lack of QoS guarantees) due to different networks coexistence. In this regard, spectrum sharing techniques such as Licensed Shared Access and Spectrum Access System could be suitable solutions for mMTC applications since they can provide better interference management. Other interesting spectrum sharing solutions include NOMA and D2D communication [97]. This section focuses on transmission scheduling and resource allocation techniques as potential solutions to deal with insufficient spectrum.

To enable low latency MTC, MTDs can perform contention-based access because it offers smaller delay and signaling overhead than traditional schemes. This is because MTDs transmit packets on a randomly selected resource without having any specific scheduled resources [98]. However, many devices trying to access the network results in situations where the number of requests exceeds the available resources. In such scenarios, it is important to know the devices prone to communication failure, e.g, due to bad channel conditions, and expected failure duration. This knowledge permits to flexibly allocate the resources among the MTDs with better conditions, provide scalable transmission time interval and guarantee QoS, e.g., minimizing outage probability. Due to the scarce network resources, the scenario where the BS allocates the channel resources to all the MTDs in the network might be impractical [81]. Instead, aggregators can incorporate intelligent functionalities such as different type of scheduling mechanisms to improve network performance [77], [99]. Notice that the limited number of services, e.g., voice, video and web, and QoS requirements supported by LTE make the traditional scheduling policies not suitable for MTC where the channel quality and QoS requirements are equally important [100]. For these reasons, novel solutions have been proposed to optimize the MTDs selection task across the network and improve data aggregation and transmission.

Two scheduling schemes are proposed in [77] to be implemented by aggregators: RRS and CRS. The authors use SG tools to show that CRS and RRS schemes achieve similar performance as long as the aggregator's available resources are not limited. On the other hand, CRS outperforms RRS when the number of MTDs requesting service exceeds the available channels. Later, these scheduling mechanisms were extended in [101], [102] under NOMA and imperfect SIC. The aforementioned schemes consider a fixed number of available resources at the aggregator and do not address the MTDs heterogeneity and their variable QoS (channels are assigned based on the received signal strength). In contrast, authors in [100] introduce two scheduling schemes for uplink MTC, which consider both channel conditions and maximum allowed delay of each device requesting service to deal with QoS demands. The former reduces the outage probability while the latter allows saving power by setting the device to sleep mode until the next transmission takes place.

After optimal MTDs scheduling, an interesting question is how to efficiently distribute the available resources among the selected devices based on goals such as throughput maximization [103], interference minimization [104], etc. An interference-aware subcarrier allocation algorithm is investigated in [105] to maximize the connectivity of

mMTC devices (sensors and actuators) subject to QoS requirements of eMBB devices (monitoring cameras) in an industrial wireless network. The maximum interference that each subcarrier can support is calculated. Then, authors determine the MTD pair with the least interference to the subcarrier and estimate the access property according to whether the MTD pair's QoS is satisfied. When the accumulated interference caused by the MTD pair is greater than the maximum interference limit that the subcarrier can sustain, the subcarrier will not be accessible to other MTDs pairs anymore. Meanwhile, authors in [91] suggest to dynamically allocate channels to the MTDs while considering the SNR, queuing delay, QoS requirements, and the pending number of devices in a class. The simulation results show that resource allocation and aggregation bring significant improvement in outage probability, energy efficiency, and system capacity. Finally, rate control is another resource allocation strategy that can be exploited to meet stringent reliability requirements. Authors in [106] propose a joint optimization of the rate control in the network layer and transmission rate in the physical layer in a D2D scenario. This approach avoids data imbalance and, therefore, packet drop at the transmitter due to limited queue buffering capability, which leads to unacceptable latency and unreliable transmissions. The proposed algorithm is not constrained to D2D-relay networks, but it can extend to different application scenarios such as energy harvesting.

2.3 Stochastic geometry

Among the most popular analytical approaches for wireless networks analysis, we can mention scaling laws, fixed geometry based analysis, graph theory (percolation) and SG. The problem of finding scaling laws for large wireless networks with randomly distributed nodes was first investigated in [107]. This approach describes how, both local and global, network connectivity properties scale with various network parameters [108]. However, the complex nature of large wireless networks with stochastic nodes distribution makes the derivation of exact results intractable, and design insights are extremely difficult to obtain [109]. Analysis based on fixed geometry provides concrete results but lacks generality since it does not fit to the network behavior under different spatial realizations. Moreover, spatial configurations may change over an infinite number of possibilities; thus, it is impossible to design wireless systems for each specific configuration [110]. In graph theory, a graph consists of number of vertices and edges, where an edge is an association between two vertices. In the wireless network context, a vertex is equivalent to a node and an edge is a link between two nodes; thus, any network can be modeled mathematically as a graph[1], e.g, mobile ad-hoc networks (MANETs) [112]. On the other hand, SG provides tractable models and accurate performance bounds to characterize and better understand dense wireless networks' operation with randomly distributed nodes. Depending on the network type and the MAC layer behavior, SG permits to abstract nodes' position to a suitable PP that captures the network properties. Modeling all active nodes' locations is crucial since it determines the SIR at the receiver side. Notice that the strength of received signals depends heavily on the distances between transmitters and receivers. Thus, many quantities of interest,

[1]Graphs can be algebraically represented as matrices; thus, network study can be automated through algorithms [111].

e.g., aggregated interference, outage probability, achieved/transmission data rate and bit error probability, can be evaluated by averaging over all network topologies seen from a "*typical point*" weighted by their probability of occurrence [113]. This abstraction level helps designers to optimize and modify important network parameters efficiently. Moreover, the average results provide the generality missing in fixed geometry-based approaches.

The *typical* point concept is essential in PP theory, and it often refers to the typical user, typical receiver, typical vehicle, etc, in the wireless communications context. If the total number of points is finite, such typical point comes from selecting one of the points uniformly at random. Notice that nothing "typical" relates a point selected in a deterministic way; moreover, it is impossible to select a point uniformly from an infinite set. Accurate results require many realizations of the PP since no point is typical in a single realization, and every point inside the PP must have the same probability of being selected [114]. If the PP is stationary[2] and ergodic[3], we can generate the typical point statistics by averaging those of each point in a single realization, observed in a sufficient large observation window. Notice that stationarity is not sufficient to obtain the statistics of the typical point by considering many points in a single realization; but ergodicity is also vital. This reflects the "average" nature of the typical point concept. In other words, we may find that the "typical person" in any country is 1.70 cm tall, which means that if we measure every person height from a large population sample, we would obtain that average height, but this does not mean that an individual with that exact height exists. Thus, for any stationary PP, we obtain the typical point by conditioning on a point existing at a certain location (Slivnyak's theorem [114]), without loss of generality, usually the origin to achieve mathematical tractability, and averaging over the PP. Contrary, in the non-stationary case, the typical point at a particular location may show different statistical properties than the typical point at a different position. This notion of typical point has important implications for efficient cellular network transmission schemes, such as NOMA, beamforming, and BS cooperation, in both downlink and uplink [116].

2.3.1 Poisson point process

The most widely used approach for modeling the network geometry is the Poisson PP (PPP), mainly due to its analytical tractability. In a PPP, the number of points located in two (or more) non-overlapping (disjoint) regions is independent, and random following a Poisson distribution. In other words, the points show little or, ideally, zero interaction. If that is not the case, non-Poisson models would be more suitable for representing the particular scenario.

To define a PPP on some mathematical space, only a single mathematical object is needed. This object is a type of *measure*[4] from measure theory called the mean measure

[2]Statistical parameters of an underlying process do not vary over space (invariant under translation).

[3]A stationary process is said to be ergodic if one can obtain all its statistical characteristics from any of its single random realizations. In other words, regardless of what the individual samples are, the collection of samples must represent the whole process [115].

[4]A measure on a set is a function that assigns a non-negative real number to a subset of the set.

or intensity measure, denoted as Λ. This intensity measure is the *first moment* of a PP (analog to the expected value of a random variable) and can be interpreted as the average number of points located in a region of the underlying space [114]. If the intensity measure is a function of the location, then it is called inhomogeneous (non-uniform) PPP. Thus,

$$\Lambda(A) = \int_A \lambda(x, y)\, dx\, dy, \tag{1}$$

where A is in general a d-dimensional bounded volume, $\mathbb{E}[\Phi(A)] = \Lambda(A)$, and $\lambda(x, y)$ is a locally integrable positive function known as intensity. As illustrated case, we consider $dx\, dy$ as the 2-dimensional volume element (area element), but it could be any dimension. Instead of $\lambda(x, y)$ and $dx\, dy$, one could write, in (two-dimensional) polar coordinates $\lambda(r, \theta)$ and $rdrd\varphi$, where r and φ denote the radial and angular coordinates respectively. For any collection of disjoint bounded sets $A_1, \ldots, A_k$, an inhomogeneous PPP with intensity $\lambda(x, y)$ has the finite-dimensional distribution

$$\mathbf{P}\{\Phi(A_1) = n_1, \ldots, \Phi(A_k) = n_k\} = \prod_{i=1}^{k} \left(\frac{(\Lambda(A_i)^{n_i}}{n_i!} \mathrm{e}^{-\Lambda(\mathrm{A_i})} \right), \tag{2}$$

where $\Phi(A_k)$ denotes the number of points in the region $A_k \subset \mathbb{R}^2$. One efficient method to simulate an inhomogeneous PPP [117], [118] implies generating first a homogeneous one with intensity value λ', which is an upper bound of the distance-dependent intensity function $\lambda(x, y)$. Then suitably transform the points according to deterministic function; this is, to thin[5] the homogeneous PPP with the thinning probability function $p(x, y) = \lambda(x, y)/\lambda'$. Notice that depending on the specific intensity measure, non-homogeneous PPPs can model either repulsive or cluster process. This PP is appropriate for modeling the pico-BSs installed around the macro-cell boundaries to improve the network coverage. The Cox process is an example of PP belonging to this group. Specifically, the Poisson line Cox PP has found interesting applications to study wireless communication networks in cities, where the streets correspond to Poisson lines (Vehicular networks) [120], [121].

When the intensity does not vary over the underlying space (independent of the location), the resulting PP is called a homogeneous (uniform) PPP. The following finite-dimensional distribution can represent these properties

$$\mathbf{P}\{\Phi(A_1) = n_1, \ldots, \Phi(A_k) = n_k\} = \prod_{i=1}^{k} \left(\frac{(\lambda|A_i|)^{n_i}}{n_i!} \mathrm{e}^{-\lambda|\mathrm{A_i}|} \right), \tag{3}$$

where $\Phi(A_1), \ldots, \Phi(A_k)$ are independent Poisson random variables of parameters $\lambda|A_i|, \ldots, \lambda|A_k|$, respectively, and $\mathbb{E}[\Phi(A)] = \lambda|A|$. An illustration of a uniform and non-uniform PPP in $\mathbb{R}^2$ is shown in Figure 4. Notice that in contrast to the uniform PPP, the non-uniform PPP intensity is periodic along the x-axis, while it decreases along the y-axis.

Other appealing properties exploited by network designers include that the sum of PPPs is still a PPP, the probability generating functional (PGFL) [114] is known in closed-form, and the distance distribution among the nodes, namely, the distance to the n-th neighboring node is known.

[5]The thinning operation refers to creating a new PP from an underlying PP by removing or retaining points according to some probabilistic rule [119].

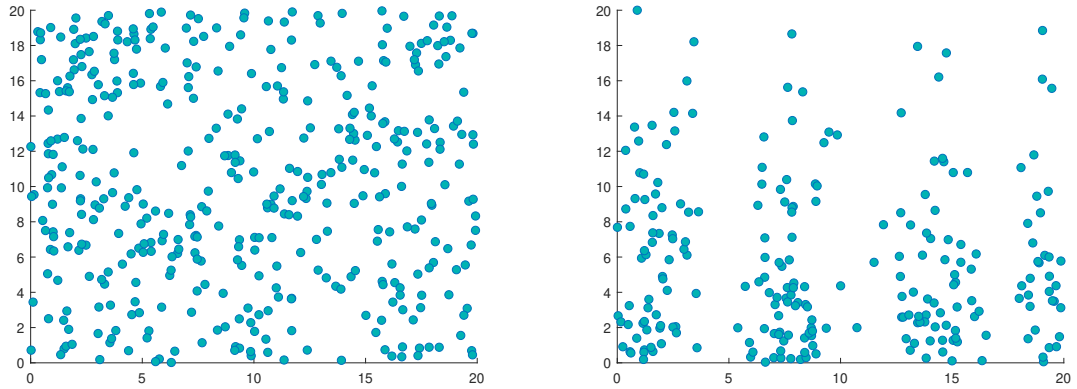

Figure 4. Example of an homogeneous PPP with $\lambda = 1$ (left), and an inhomogeneous PPP with $\lambda(x, y) = 2\exp(-y/6)(1 + \sin x)$ (right) on $[0, 20]^2$.

2.3.2 Non-Poisson point process

While models based on PPP have provided important insights on wireless networks performance over the last years; empirical evidences[6] indicate that in current cellular networks, the BSs positions lies somewhere between completely random (as modeled by PPP) and deterministic. This is because the BSs deployment depends on network topology, network planning, and the geographical region type. Even in cellular networks where a PPP models BSs positions, active users served in the same time-frequency resource block do not form a PPP. For instance, in the heavily loaded BSs case, the user PP seems to follow a Ginibre PP [123]. Moreover, the PPP implies uncorrelated node's positions; therefore, it may not be suitable to model networks with interference management techniques, where repulsion or attraction among the nodes exists [124]. Thus, a single PP model is insufficient to capture the variety of node densities, propagation conditions, and deployment structures in all scenarios. These limitations motivate more realistic models based on non-Poisson processes that accurately fit practical deployments. For non-Poisson processes, conditioning on a point being at a certain location changes the PP statistics. This is because the number of points in disjoint regions may be dependent on each other. Therefore, mathematical tractability is hard to achieve in most cases.

In many practical scenarios, PPs with repulsive nature (points negatively correlated) can model the set of nodes that transmit simultaneously over the same channel. A PP with repulsion (regular PP) arises when points cannot approximate other than a certain minimum distance, e.g., two contiguous BSs cannot be randomly close in actual cellular networks because of physical constraints and MAC scheduling. The following PPs have these repulsive features:

- **Matérn hard-core process (MHC):** Type I and II Matérn hard-core processes are the PPs of choice to model concurrent transmitters in dense wireless networks operating carrier sense multiple access protocol that imposes distance constraints

[6]For instance, by fitting a real BSs deployment data-set of the operator Vodafone in rural and urban zones in the UK, authors in [122] show that the Strauss and the Poisson hard-core processes provide better models.

between simultaneous transmitters [125], [126]. Both types are constructed from a parent PPP of intensity $\lambda > 0$. In the type I process, all nodes with a neighbor within a fixed distance δ are thinned; whereas in the type II process, a random mark is assigned to each node, and a node is thinned only if another node with a smaller mark exists within a distance δ. This is an example of a *dependent* thinning operation [119].Then, in contrast to what happens for an independent PPP thinning, the resulting MHC process is not a PPP. These processes are difficult to analyze since their PGFLs do not exist. Additionally, both PPs behave differently [127]. For type I, the excess interference relative to the PPP increases exponentially in λ and δ (for power-law path loss), while for type II, the excess interference never exceeds 1dB, regardless of the path loss model.

- **Determinantal point process (DPP):** is a soft-core PP with adaptable repulsiveness [128]. The Ginibre point process (GPP) is a particular case of DPP that served in [129] as a model for sensors and gateways locations in a wireless sensor network with energy harvesting. Specially, the β-GPP, which is a thinned and re-scaled GPP, where $0 < \beta \leq 1$ is the retaining probability, serves to model to BSs locations in cellular networks [130].

- **Poisson hole process (PHP):** is constructed using two independents PPPs Φ_1 and Φ_2 with densities λ_1 and λ_2, respectively, where $\lambda_2 > \lambda_1$. Φ_1 represents the hole centers, while Φ_2 constitutes the baseline process from which the holes are formed. In other words, all the points located inside a circle of radius D around each $x \in \Phi_1$ are removed to form the holes. Thus, the points retained in Φ_2 after forming the holes constitute the PHP Ψ_H, which can be mathematically defined as [131]

$$\Psi_H = \{x \in \Phi_2 : x \notin \bigcup_{y \in \Phi_1} \mathcal{B}(y, D)\}, \tag{4}$$

  where $\mathcal{B}(y, D)$ is a circle of radius D centered at y and mimicking a hole. This PP is suitable for applications such as cognitive radio, where the main objective is to improve spectrum utilization by allowing unlicensed secondary users to use licensed spectrum as long as they do not cause excessive interference to the licensed primary users. Thus, it is important to create exclusion zones (holes) around primary users, where secondary transmissions are not allowed [131], [132]. The PHP has also been used to model inter-tier dependence in the BS locations in heterogeneous cellular networks (HCN), in which case, small cells form the PHP [133]. In [134], a PHP formulation allows integrating D2D and cellular networks by creating exclusion zones around cellular users and protect their communication from the interference coming from D2D transmissions. Note that although the exact characterization of interference experienced by a typical node in the PHP is unknown; several tight upper and lower bounds on the Laplace transform are provided in [131].

On the other hand, in many practical wireless scenarios, the transmitters form clusters due to geographical factors, e.g., indoor access points and groups of nodes moving in a coordinated manner. Besides, MAC protocols can induce clustering phenomenon among transmitters [135]. Thus, clustered PPs can suitably model such correlated transmitters' locations. Moreover, they accurately model ultra-dense 5G HCNs, which include macrocells, picocells and femtocells [136–138]. Any cluster process is generated

by taking a parent PP and a daughter PP per each parent point, and translating the daughter processes to their parent's positions. The cluster process is then the union of all the daughter points. If the parent process is stationary, and the daughter processes are independent among themselves and also from the parent process, and have the same distribution, the procedure is called homogeneous independent clustering. Thus, only one cluster represents the statistics of the whole process. Moreover, if each cluster is itself a finite PPP, the resulting process is called a doubly PPP [114]. These important concepts will help the reader understand some of the system model's assumptions in the next chapter. The following PPs present these attraction features:

- **Thomas cluster process (TCP):** is a stationary and isotropic Poisson cluster process generated by a set of daughter points (random in number) independently and identically distributed according to a symmetric normal distribution with zero mean around each parent point PPP [139].

- **Matérn cluster process (MCP):** is a doubly Poisson cluster process, where the daughter points are uniformly distributed on the ball centered at each PPP parent point [114], [140]. Modeling based on MCP can capture both clustered and bounded properties of D2D communications in urban areas as in [141].

- **Gauss-Poisson process (GPP):** is a Poisson cluster process with homogeneous independent clustering. Each cluster has one or two points, with probabilities $1-p$ and p, respectively. If a cluster has one point, it is located at the position of the parent. If a cluster has two points, one of them is at the position of the parent, and the other is randomly distributed around the parent with some probability density function (PDF) [114]. Author in [135] propose the GPP as a model for wireless networks that exhibit clustering behavior and derive the SIR distributions for cooperative and non-cooperative transmission schemes.

Figure 5 shows the PP taxonomy. The PPP is the PP with zero interaction among the points. Moving to the right, points attract each other, which result in clustered processes. Meanwhile moving to the left, points start to repulse each other, which leads to regular processes. Figure. 6 illustrates snapshots of two PPs realizations, namely, DPP and Thomas cluster process. Notice that under certain conditions, combinations[7] of these simple PPs might produce an intractable PP as in [142].

2.3.3 Spatial statistics for point processes

In the previous subsections, we showed that many PPs could be used for modeling different types of communication networks with diverse characteristics. Given all the PPs mentioned earlier, an interesting question is how accurate they can model practical deployments. Moreover, in some scenarios [142], operations on PPs such as dependent thinning result in a PP from which it is impossible to analytically evaluate performance metric, e.g. success probability. In these cases, a detour is taken, and the underlying PP is approximated by simpler ones (PPP and TCP) in order to benefits from their

[7]Combinations in this context refers to operation among PPs such as superposition or mappings such as indicator functions.

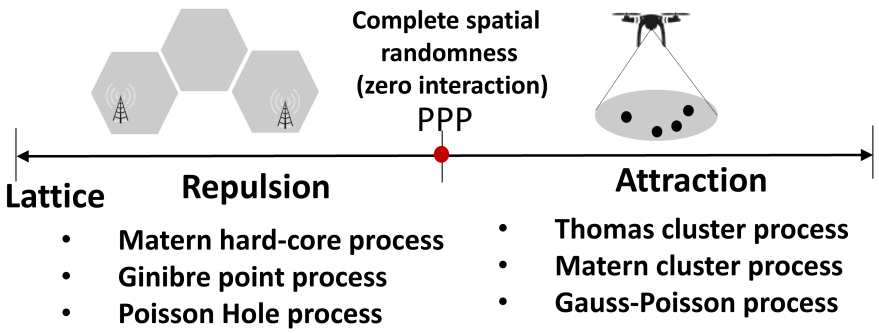

Figure 5. Stochastic dependency among PPs.

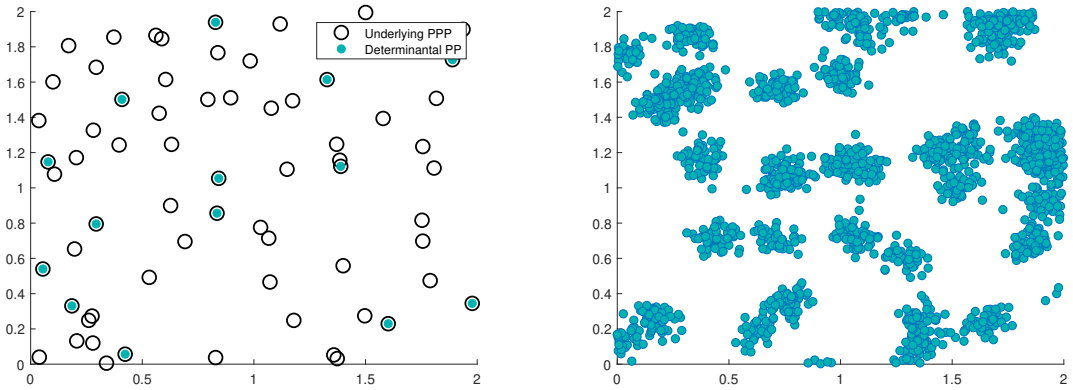

Figure 6. Comparison between repulsive process (Determinantal PP on the left) and clustered process (TCP on the right).

explicit PGFL expressions. Thus, classical spatial statistics are considered for testing these models' goodness-of-fit and comparing different PPs structures. At this point, we find useful to make a slight distinction between points and events. The former refers to geometrical positions in the plane, while the latter refers to points where "something" happens, e.g., the interferers' positions in a wireless system.

The contact distribution function or empty space function denotes the shortest distance from the given fixed location u to the nearest point of of the PP (nearest event). Thus, it provides information about the empty space between points. It is defined as [143]

$$F(r) \triangleq \mathbb{P}(\Phi(\mathcal{B}(u,r)) > 0), \tag{5}$$

where $\Phi(\mathcal{B}(u,r))$ denotes the number of points within the ball of radius r centered at the reference point u that does not belong to the original PP. For a stationary PP, any arbitrary point in $\mathbb{R}^2$ can be treated as reference point; thus, the origin typically offers more tractability. Notice that if we denote $||u-\Phi||$ as the shortest distance from the given location u to the nearest point in Φ, then $||u-\Phi|| \leq r$ holds if and only if $\Phi(\mathcal{B}(u,r) > 0)$; thus, the contact distribution function matches the cumulative distribution function (CDF) of the distance from the location u to the nearest point. This is an important statement that can be exploited to test complete spatial randomness by comparing the PDF of the distance distribution from the origin to the nearest point of any PP with the theoretical $F(r)$ corresponding to the PPP. Moreover, (5) is more

powerful at detecting deviations from complete spatial randomness in the direction of clustering [144]. If the events are clustered, the $F(r)$ function will rise slowly at first but more rapidly at longer distances; this is because a good portion of the study area is empty; therefore many random points locations are at longer distances from the nearest event in the pattern.

The nearest-neighbor distance distribution function is a different concept from the contact distance distribution. In this case, the goal is to determine the distance from a point of the process, $z \in \Phi$, to its nearest neighbor (event-event distance distribution) defined as [114]

$$G(r) \triangleq \mathbb{P}(||z - \Phi \backslash \{z\}||), \qquad z \in \Phi. \tag{6}$$

Notice that the contact distance becomes the nearest-neighbor distance when the reference point is part of the original PP. Moreover, for the PPP, both functions are identical [145]. Authors in [139] provide the contact distance and the nearest-neighbor distribution functions for the TCP. For the latter, two cases are analyzed: *i*) the reference point is chosen uniformly at random from the TCP, and *ii*) it is a randomly chosen point from a cluster chosen uniformly at random from the TCP.

The previous measures are only based on the nearest neighbor and have the drawback that nearest-neighbor distances can be arbitrary small relative to other distances in the point pattern; thus, they can mask important structures in the pattern depending on the study area dimensions. A common approach around this problem consists of using the Ripley's $\mathcal{K}$ function [143] instead. This is a second-order statistic defined for stationary PPs that carries important information about the dependence or interaction between different points of the process. Moreover, it counts the mean number of events within distance r of a given event in the PP, excluding the point itself. In other words, it is used as a measure of repulsiveness/clustering. Specifically, compared to the completely spatial random PPP, a repulsive PP model has a smaller $\mathcal{K}$ function, while a clustered PP model has a larger $\mathcal{K}$ function, in which case, more events are being counted. Formally, for a stationary and isotropic PP Φ with intensity λ, the $\mathcal{K}$ function is defined as [114], [146]

$$\mathcal{K}(r) \triangleq \frac{\mathbb{E}^{!0}[\Phi(\mathcal{B}(0,r))]}{\lambda}, \tag{7}$$

where $\mathbb{E}^{!0}(\cdot)$ is the expectation with respect to the conditional probabilities of the Φ events given that a point (the typical point) is observed at a specific location (reduced Palm distribution of Φ [147]), and $\mathcal{B}(0,r)$ is the ball centered at origin with radius r. For instance, this metric is utilized in [148] to examine whether simulated DPPs fit real BS deployments in two major US cities.

In many situations, we are interested in modeling the interference; thus, only the transmitters' PP is relevant. Note that the interference is not only determined by the nodes' spatial configuration, but also by the MAC scheme, which performs a thinning operation on the whole set to produce the transmitters' set. Due to its nature, in most wireless scenarios, the interference PP deviates from the simple PPP; thus, the need for non-PPP becomes inevitable. The limited analytical tractability of non-PPP makes difficult, and often impossible, to obtain closed-form expressions for network performance. This is because Campbell's theorem [114] does not hold for non-PPP. To overcome this issue, authors in [116, 123] apply the pair correlation function concept defined in [143] as

$$g(r) \triangleq \frac{1}{2\pi\, r} \frac{d}{d\, r} \mathcal{K}(r), \tag{8}$$

which is critical to approximate complex models by simpler and more tractable ones. This is, a simple PP can approximate any complex PP by performing a proper match of the respective intensities using the pair correlation functions concept. This statement can be formulated as follow. If we consider the interference PP Φ_I of general intensity λ, we would like to find a PPP Φ_{PPP} such that for all f:

$$\mathbb{E}^{!0} \sum_{z \in \Phi_I} f(z) \equiv \mathbb{E} \sum_{z \in \Phi_{\text{PPP}}} f(z). \tag{9}$$

Applying Campbell's theorem and its Palm version on the right and the left side, respectively, (9) boils down to

$$\lambda \int_{\mathbb{R}} f(z) g(||z|| \sqrt{\lambda}) dz \equiv \int_{\mathbb{R}} f(z) \lambda_{\text{PPP}}(||z||) dz, \tag{10}$$

which holds if $\lambda_{\text{PPP}}(r) = \lambda g(r\sqrt{\lambda})$. The idea is to introduce a new PP such that the network seen by a user at the origin is probabilistically equivalent (in terms of PDF) as the network seen by the typical user of the original PP. This is easily understood when realizing that the typical user sees the network through the distance from the serving BS and the corresponding interferers. Notice that a PPP is a natural choice as approximation, but in principle, any PP with intensity function λ_{PPP} can be used. Also notice that estimating the intensity of the approximated PP is based on the same principles as the mean and variance or any PDF is estimated in classical statistics. This is, we could obtain the curve corresponding to the pair correlation function of the underlying PP via Monte Carlo simulation and use function-fitting tools in MATLAB to produce a suitable function that mimics its behaviour. Interestingly, we realize that (9) holds certain similitude with the mean interference in wireless networks since $f(z)$ can be thought as a path loss function; thus, we can obtain general expressions for the mean interference by using the reduced second moment measure $\mathcal{K}(r)$ and combining (8), (9) and (10) as in [149]. Others methods to test PP models with practical examples are analyzed in [145].

All distance functions discussed in this section are affected by the edge effect. This issue arises from the fact that events near the edge of the study area tend to have higher nearest-neighbor distances even though they might have neighbors outside the study area closer than any inside it. To remove these edge effects, the PPs must be simulated on an extended version of the simulation window to include events that are not counted as part of the actual process but are needed to account for those distances to events close to the area's boundaries of interest. Moreover, if the study area (sampling window) is large enough, its effect can be neglected [150]. Edge effect is a more complicated topic that cannot be bypassed when analyzing point patterns but goes beyond this thesis' scope; thus, the reader can obtain more information in [151], [152].

Using any of the statistics presented in this section should be sufficient to pick a suitable PP that captures a wide range of real-world deployments characteristics since they reveal details on the range and strength of correlation in the pattern. However, in practice, it is not trivial to recognize a suitable model for each deployment. In most practical applications, some prior information often supports the model choice. For instance, data collected from the environment might show certain temporal-spatial correlation among nodes, in which case clustered PPs could be the first-trial option. However, a more detailed analysis may indicate that the modeling has to be polished. In general,

the model must be accurate and simple enough that both parameters estimation and simulation are still attainable. The first glance in the analysis of spatial PPs should test the complete randomness assumption. Results derived from this step and some visual inspection of the points distribution in the area might lead to conclusions such as whether the pattern is stationary or non-stationary, and clustered or regular. Moreover, every modeling approach should start with the classical models presented in Section 2.3.1 and Section 2.3.2, since they can easily be fitted and simulated. If these PPs result in poor models, they can even be relaxed, for instance, by choosing a non-Poisson parent process for a cluster process or by including hard cores, i.e., minimum inter-point distances. Any of these modifications should keep the model simple to be simulated [145].

2.3.4 Related works

We can refer to countless works where SG has played an important role in describing scenarios where it would have been impossible to obtain qualitative results and performance trends with traditional modeling tools. For example, in [153], the authors use an SG approach to quantify the performance of multi-hop massive IoT networks under three different packet forwarding schemes in terms of the average successful packet progress made per unit area. Moreover, a unified study of large-scale IoT spatio-temporal performance can be carried out by combining SG and queuing theory [154]. This framework allows designers to realize solutions based on combinations of temporal traffic intensity and spatial device density to avoid network inestability. For instance, authors in [155] develop a novel spatio-temporal mathematical framework using SG and queueing theory to study the performance of radio access channel procedure in challenging scenarios where a massive IoT system coexists with traditional cellular systems[8]. Meanwhile, authors in [157] perform a complete study of LoRa scalability considering various channel parameters and multiple gateways using tools from SG. Later in [158], SG is also used to evaluate networks' scalability by modeling the effect of interference resulting from the imperfect orthogonality of the spreading factors. An analytical framework based on SG is proposed in [159] to model the outage probability when several replicas of the same packet are transmitted from heterogeneous sources with correlated deployment locations in LPWA IoT networks. The correlation is captured by Poisson cluster PPs that contain the position of nodes reusing radio resources with a similar or different code as the transmitter of interest. Authors in [113] and [160] survey different PPs to describe multi-tier and cognitive cellular wireless networks, and present several SG approaches to analyze network performance and interference management techniques in these types of scenarios. Modeling, analysis, and optimization of grant-free NOMA in mMTC via SG is performed in [161]. Finally, the vital role of SG as an analytical tool for performance evaluation of 6G networks is analyzed in [162].

[8]To learn some of the challenges in the coexistence of massive IoT and traditional cellular networks, see [156].

2.4 The meta distribution of the SIR

A key metric of interest in interference-limited networks is the traditional success probability given a SIR threshold θ, $p_s(\theta) = \mathbb{P}(\text{SIR} > \theta)$, at a "*typical receiver*" in the network, obtained by averaging over the channel fading, the channel access scheme and the PP. Thus, the success probability is the result of spatial averaging over the entire PP, and only provides users' average performance. In other words, it does not reveal how concentrated the link success probabilities are considering different users; therefore, it is not possible relying on this metric to distribute the transmit resources across the network with QoS guarantees.

A simple experiment allows us to understand above issues better. As an illustration, consider Poisson bipolar networks and slotted ALOHA medium access protocol with transmitting probability p. The potential transmitters form a PPP with intensity λ and each one has a dedicated receiver at distance R in a random orientation[9]. This is a typical model for self-organizing wireless communication networks such as MANETs in which mobile devices dot not rely on any BS [111]. For Poisson bipolar networks, the success probability expression under Rayleigh fading is provided in [163] as $p_s = \exp\left(-C\lambda\theta^{\delta}p\right)$, where C is a constant that depends on the link distance R and path loss exponent α. Notice that if we keep λp constant for a fixed θ, p_s does not change. Then, we show in Figure 7 the individual link reliabilities histogram for constant $\lambda p = 1$ (constant p_s) while changing p to 0.8, 0.4, 0.1 and 0.01. The red cross specifies the average of all link reliabilities, p_s, which remains constant at 0.84 in all cases. Clearly, the distribution of link reliabilities changes significantly, even with constant p_s. Consequently, it is important to measure the fluctuation of the link reliability around p_s to fully characterize the network's performance in terms of connectivity, end-to-end delay, per-device reliability, etc, since a performance distribution contains much more information than just its mean.

We center our attention on random variables of the form

$$P_s(\theta) \triangleq \mathbb{P}(\text{SIR} > \theta|\Phi), \tag{11}$$

where the conditional probability is taken over the fading and the channel access scheme and given the nodes' position for a particular realization of the network. In general, the moments of the conditional success probability, $M_b(\theta) \triangleq \mathbb{E}(P_s(\theta)^b)$, carry enormous importance, as we will show later. Particularly, the -1-st moment is known as the mean local delay, and it is defined as the average number of transmissions attempts until a packet is successfully received if the transmitter is constantly transmitting [164]. The first moment is interpreted as the standard (average) success probability, $p_s(\theta) = \mathbb{E}[P_s(\theta)]$; and the variance, $\text{Var}(P_s) = M_2 - M_1^2$, quantifies the performance difference among all the devices in the network, i.e., network's fairness. For example, by analyzing these two metrics, authors in [165] provide insights to determine the most efficient operating antenna configurations for URLLC applications in 5G cellular networks with coexisting sub-6GHz and mm-Wave transmissions. This analysis shows that as the number of antenna elements in a hybrid spectrum network increases, the reduction in the variance of reliability is noticeable.

[9]By the displacement theorem [114], the receivers PP is also a PPP. Thus, the Poisson bipolar network consists of two dependent PPPs.

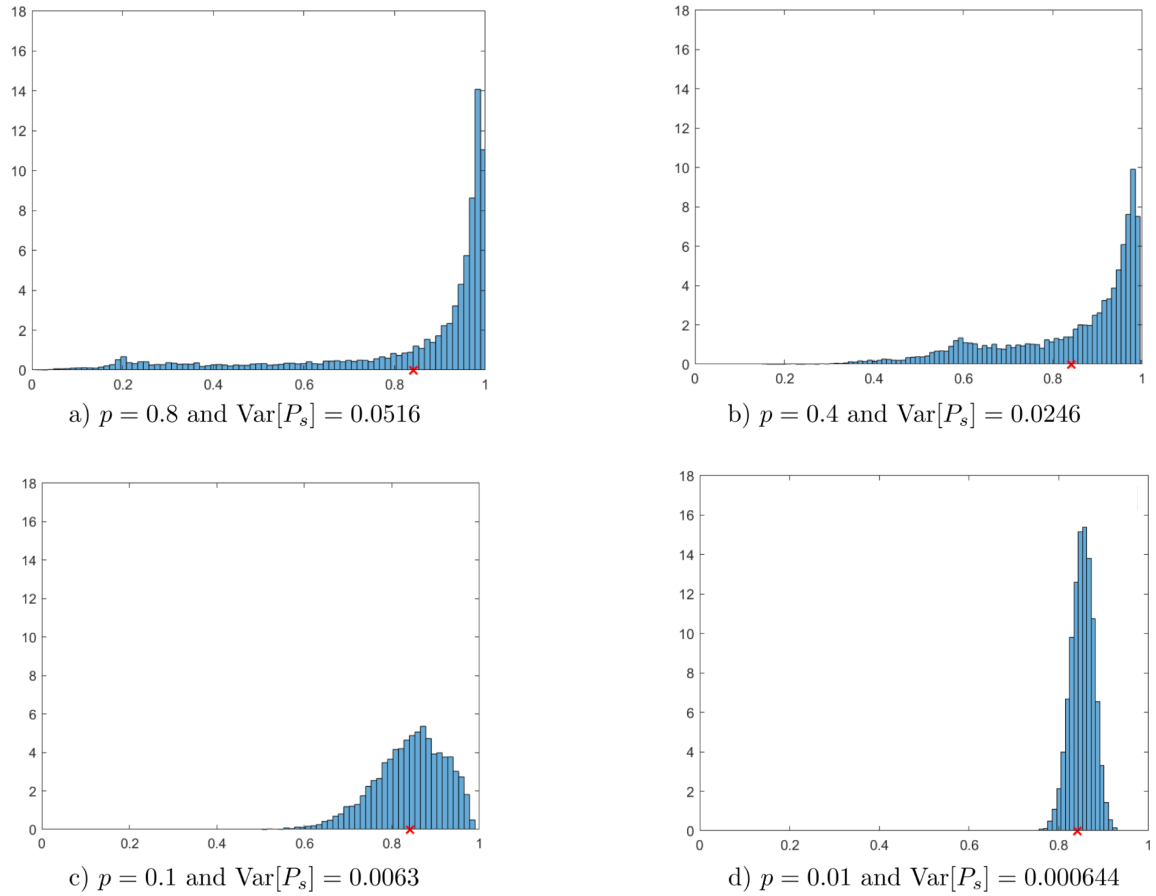

a) $p = 0.8$ and $\mathrm{Var}[P_s] = 0.0516$

b) $p = 0.4$ and $\mathrm{Var}[P_s] = 0.0246$

c) $p = 0.1$ and $\mathrm{Var}[P_s] = 0.0063$

d) $p = 0.01$ and $\mathrm{Var}[P_s] = 0.000644$

Figure 7. Link reliability histogram and traditional success probability $p_s(\theta)$ (red cross) in Poisson bipolar network with ALOHA. The histogram of the empirical probability density function of the link success probability in a Poisson bipolar network with ALOHA channel access for $R = 1/3$, $C = 0.5483$, $\theta = -10$ dB and $\alpha = 4$.

The intention is then to find the two-parameter complementary CDF of $P_s(\theta)$, defined as [166]

$$\bar{F}(\theta, x) \triangleq \mathbb{P}(P_s(\theta) > x), \tag{12}$$

where $x \in [0, 1]$ refers to the target reliability level. Due to the ergodicity of the PP, one can understand $\bar{F}(\theta, x)$ as the fraction of links or users that achieve an SIR θ with a probability of at least x [166]. This is a new fundamental performance metric called the MD of the SIR, which was first introduced in [166] in the context of Poisson bipolar and cellular networks. Notice that the MD isolates the randomness produced by the small-scale fading from the location of interferers [167].

2.4.1 Mean local delay

Critical MTC applications require transmission with very low latency, below 1 ms, [51]. The per-link delay consists of four types of delays: the processing delay, the queueing delay, the transmission delay, and the propagation delay. Due to the high-performance central processing units produced nowadays, the processing delay is negligible in most

wireless network applications compared to the queueing delay and the transmission delay. Moreover, the propagation delay can also be insignificant since radio signals propagate at close to the speed of light. The main component of the transmission delay is the retransmission delay, which is closely related to the number of retransmissions of a packet, often called local delay [164]. The local delay, denoted by L, is defined as the number of transmission attempts needed until a packet is successfully received (decoded) over a wireless link. Thus, the mean local delay can be written as

$$\mathbb{E}[L] = \mathbb{E}[\mathbb{E}[L|\Phi]] = \mathbb{E}\left[\frac{1}{P_s(\theta)}\right] = M_{-1}, \tag{13}$$

where the inner expectation is obtained by averaging over the fading and the MAC protocol if it exists. This is an important network performance metric that it is finite when certain network parameters, such as the SIR threshold and the medium access probability, are below specific thresholds [168]. In these situations, the fraction of nodes that experience such related long delays is negligible . It is known, for instance, that highly mobile networks provide enough time diversity to keep the local delay finite [169]. The mean local delay may show a phase transition called wireless contention phase transition [168]. In this case, it becomes infinite at some critical value of a network parameter, i.e., a successful packet transmission requires infinite time slots, which means there is a considerable number of links with long delays [169]. More interestingly, L follows a geometric distribution with parameter P_s given in (11)

$$\mathbb{P}\left(L = \tau \mid \Phi\right) = \left(1 - P_{\mathrm{s}}\right)^{\tau - 1} P_{\mathrm{s}}, \quad \tau \in \mathbb{N}. \tag{14}$$

For ergodic PPs, we can obtain that [116]

$$\mathbb{P}\left(\mathbb{P}\left(L \leq \tau \mid \Phi\right) > x\right) = \mathbb{P}\left(1 - (1 - P_{\mathrm{s}})^{\tau} > x\right) = \bar{F}_{P_{\mathrm{s}}}(1 - (1 - x)^{1/\tau}), \tag{15}$$

which states the fraction of users that succeeds decoding the received signals in at most τ time slots with probabilities larger than x. For example, with $x = 0.90$, $\bar{F}_{P_{\mathrm{s}}}(0.90)$ is the fraction of users that receive their desired signals successfully in the first transmission attempt (i.e., $\tau = 1$) with a probability higher than 0.90, while $\bar{F}_{P_{\mathrm{s}}}(0.68)$ is the fraction of users achieving the same goal after the second transmission attempt (i.e., $\tau = 2$) for the same target reliability, or equivalently, the fraction of users that successfully decoding the data messages in the first time slot with reliability 0.68.

Authors in [170] define the region of the activity probabilities in which the mean local delay of each tier remains finite in an HCN where the BSs activity is modeled by ALOHA. The impact of increasing the BS density on the mean local delay in a D2D communication scenario is investigated in [171]. Authors in [172] evaluate the optimal number of sub-bands in frequency-hopping multiple access and the optimal transmit probability in ALOHA that minimize the interference correlation and the mean local delay. Results reveal that if no MAC dynamics are implemented, the local delay has a heavy tail distribution which results in infinite mean local delay. Finally, authors in [173] study the effect of bandwidth partitioning on the reliability and the local delay performance in a Poisson bipolar network. It is shown that there is a finite optimum number of sub-bands that minimizes the local delay.

2.4.2 Computation tools

Direct calculation of (12) is usually infeasible or may be cumbersome because the interference PDF is hard to find except for just a few path loss and fading models[10]. Thus, different methodologies have been recently proposed in the literature to find exact or approximate closed-form expressions, or even efficient numerical computation methods, for the MD of the SIR, e.g.,

- **Gil-Pelaez approach**: Since the MD has finite support in $[0, 1]$, the problem of extracting the distribution from its integer moments boils down to solve the Hausdorff moment problem [174], [175], and the solution is unique if it exists. This method exploits the Gil-Pelaez inversion theorem [176] from the imaginary moments of the conditional link success probability, $M_{jt} = \mathbb{E}[P_s(\theta)^{jt}]$, where $t \in \mathbb{R}^+$ and $j \triangleq \sqrt{-1}$. The MD is then given by

$$\bar{F}_{P_s}(x) = \frac{1}{2} + \frac{1}{\pi} \int_0^\infty \frac{\Im[e^{-jt \ln x} M_{jt}]}{t}\, dt, \tag{16}$$

  where $\Im[\cdot]$ denotes the imaginary part of a complex number. This method has been extensively used in the literature e.g. [166], [177–183], but its main drawback resides in the fact that it involves the computation of complex numerical integrals for which the limits and step size need to be carefully selected [184], and it is a time-consuming method.

- **Binomial mixtures approach**: Using this approach, the exact MD can be obtained by evaluating

$$\bar{F}_{P_s}(x) = 1 - \sum_{k=0}^{\lfloor nx \rfloor} \underbrace{\sum_{b=k}^{n} \binom{n}{b} \binom{b}{k} (-1)^{b-k} M_b}_{\varrho_k}, \qquad \forall x \in (0, 1], \tag{17}$$

  while $\bar{F}_{P_s}(0) = 1$. The notation $\lfloor v \rfloor$ is used to denote the largest integer less than or equal to v. Notice that $M_b = \mathbb{E}[P_s(\theta)^b]$ and $n \in \mathbb{Z}^+$ refers to the number of integer moments. The larger n is, the more accurate the results become, but at the expense of high computational time, although in general it converges much faster than Gil-Pelaez approach. Notice that ϱ_k is a linear combination of the moments; thus, it can be expressed as the linear transformation $\boldsymbol{\varrho} = \mathbf{A}\mathbf{m}$, where $\mathbf{m}$ is a column vector containing the moments, i.e., $\mathbf{m} = (M_b)_{b=0}^n$, and $\mathbf{A} \in \mathbb{Z}^{(n+1)\times(n+1)}$ is defined as [185]

$$A_{bi} \triangleq \binom{n}{b} \binom{b}{i} (-1)^{b-i} \mathbb{1}(b \geq i), \qquad i, b \in \{0, 1, 2, \ldots, n\}, \tag{18}$$

  where $\mathbb{1}(\cdot)$ is the indicator function. This linear mapping is an upper triangular matrix, symmetric with respect to the antidiagonal, and needs to be calculated only once for the desired level of accuracy. An example for $n = 4$ is provided in [185].

[10] [113] reviews different techniques to bound the aggregate interference and evaluate the network performance.

Notice that this procedure avoids the need of complex operations as required in the Gil-Pelaez technique. However, high order moments are needed and they are not always feasible to compute [185]. This method was first proposed in [186], where it was also compared with Poisson mixtures. Moreover, it was later used in [182] to compute the energy MD in a wireless powered network with direct wireless energy transfer from power beacons to low-power wireless devices. Additionally, it was utilized in [180] to determine the coverage probability MD with and without line of sight propagation, for which, the first 25 moments were sufficient to obtain accurate results.

- **Euler sum approach**: With this particular method, one can reconstruct the MD with a known and bounded error by using the trapezoidal integration and the Euler sum rule. This approach was proposed for the first time in [187], and later used in [188] to compute the coverage probability in a power beacon-assisted mm-Wave ad-hoc network. Using this approach, the MD can be formulated as [189]

$$\bar{F}_{P_s}(x) \approx \frac{2^{-Q}\exp(\frac{A}{2})}{\ln^2 x}\sum_{q=0}^{Q}\binom{Q}{q}\sum_{n=0}^{B+q}\frac{(-1)^n}{\beta_n}\Re\left\{\frac{M_{-S_n/\ln(x)}}{S_n}\right\} + |\varepsilon(Q,B,A)|, \tag{19}$$

where $\Re[\cdot]$ is the real part operator; $S_n = \frac{A+j2\pi n}{2}$; $\beta_0 = 2$; $\beta_n = 1$ for $n = 1, 2, ..., q+B$; A, B and C are positive parameters used to control the accuracy[11]; finally, $|\varepsilon(Q,B,A)|$ is the approximation error, given in [189, e.q (19)] as

$$|\varepsilon(Q,B,A)| \approx \frac{1}{\exp(A)-1} + \left|\frac{2^{-Q}\exp(\frac{A}{2})}{\ln^2 x}\sum_{q=0}^{Q}\binom{Q}{q}(-1)^{N+1+q}\Re\left\{\frac{M_{-S_{N+1+q}/\ln(x)}}{S_{N+1+q}}\right\}\right|$$

- **Fourier-Jacobi approach**: The MD can also be reconstructed from its moments using truncated Fourier-Jacobi expansion. Since this method uses the information contained in the higher moments, a better accuracy is obtained; however, its convergence properties are still not completely understood [167].

- **Beta approximation**: All the numerical methods reviewed so far permit to obtain the PDF of a random variable from its Laplace transform inversion, or equivalently its moments. Notice that the moment generating function is somehow related to the Laplace transform of any random variable. But in general, it is not easy to gain insights directly from numerical results and much less apply them to obtain other analytical outcomes that help to interpret the system performance in response to variations in the design variables. Since the support of the conditional success probability $P_s(\theta)$ is $[0, 1]$, the beta distribution is a simple and more tractable choice to approximate the MD by matching the first and second moments M_1 and M_2 of $P_s(\theta)$ to those of the beta distribution, i.e.,

$$\bar{F}_{P_s}(x) \approx 1 - I_x\left(\frac{M_1(M_1-M_2)}{M_2-M_1^2}, \frac{(M_1-M_2)(1-M_1)}{M_2-M_1^2}\right), \tag{20}$$

[11]Typical values are $A = 10\ln(10)$, $B = 10$ and $Q = 20$, which guarantees an error of the order of 10^{-10} [187].

where $I_x(a,b) = \frac{1}{B(a,b)} \int_0^x t^{a-1}(1-t)^{b-1}\, dt$ is the regularized incomplete beta function, and $B(a,b)$ is the beta function. This approach reduces computational complexity because it only uses the first and second moments; therefore, it has been widely used in the literature in different scenarios, e.g., [166, 179, 181, 183]. However, one still may encounter some cases where the beta approximation does not offer a good match. For example, authors in [177] provide fine-grained performance analysis of the mm-Wave D2D communication networks where each receiver has a single antenna and its corresponding transmitter is equipped with an antenna array . It is observed that the standard beta distribution provides an excellent match for the case with severe interference, while as the number of antennas increases with narrower beams or the density of the nodes decreases, the beta approximation to the MD starts to deviate from the exact results, especially when operating at high reliabilities. This is because in mm-Wave systems, the interference behavior is different from the microwave communications due to high propagation loss, highly directional transmission, and sensitivity to blockage. Moreover, under high operation frequency the noise power cannot be neglected. To cope with this issue, the authors in [178] applied the generalized beta distribution to approximate the MD by matching the first three moments in a D2D scenario, where the randomness in the users' distribution makes both strong and weak interference scenarios possible. In general, the truncated Fourier-Jacobi expansion provides better accuracy over the simple beta approximation in this type of scenarios [167].

- **Known inequalities to bound the MD**: A simple way to lower and/or upper bound the MD is by using Markov's[12], Chebychev's and Paley-Zygmund's inequalities. In fact, the last one is particularly useful to determine the fraction of links that attain at least a certain fraction of the average performance. These bounds depend only on low-order moments of the random variable, which makes the computation faster than the numerical methods explained in this section, but the accuracy of the results is very limited. However, it might be a handy tool to obtain insights on the network performance in time-constrained design projects. This approach was used in [166] to bound the MD in a Poisson bipolar network; in [181], to analyze the performance of a cellular network with power control; and later exploited in [183] to determine the maximum density of concurrently active links that satisfies a certain outage constraint.

2.4.3 Meta distribution in non-Poisson networks

Analyzing the performance of non-Poisson networks becomes intractable in most cases since non-PPPs are difficult to simulate and have weak mathematical tractability. This problem becomes even worse in the HCNs case, where one needs to consider the intra-tier as well as the inter-tier interference and BSs in each tier may form an arbitrary stationary and ergodic PP. To cope with this issue, a simple and novel method is proposed in [190] to obtain the MD for an arbitrary non-Poisson network by shifting the MD for a PPP of reference by the asymptotic deployment gain G_0 as

$$\bar{F}^s(\theta, x) \approx \bar{F}^{\mathrm{PPP}}(\theta/G_0, x). \tag{21}$$

[12]This is used in [171] to bound the MD in a D2D scenario as the BS intensity changes.

This method is called AMAPPP, which stands for "Approximate meta distribution analysis using the PPP", and becomes extremely accurate as the SIR threshold θ decreases. Moreover, it becomes extremely handy since the moments of $P_s(\theta)$ are often computed using the PGFL based on the assumption that the nodes are deployed using a PPP, or at least it constitutes a close approximation. Notice that this approach is not equivalent to apply a shift to the SIR distribution as in [191].

Authors in [192] present another interesting case where due to the high speed in VANETs, the drivers maintain large safety distances, and consequently the PPP is not a suitable modeling tool. Thus, a novel discretization model for vehicles' locations is proposed to approximate the MD of the SIR. It is assumed that the distribution of inter-vehicle distance equals to the sum of a constant hardcore distance and an exponentially distributed random variable. In other words, the model splits the contribution to the PGFL into the near-field (modeled as a MHC process) and far-field terms (modeled as a PPP) depending on interferers' locations. The former contribution requires to average over a uniform distribution for a vehicle's location inside each interval.

Meanwhile, an analytical framework is proposed in [189] for computing the conditional coverage probability distribution given the PP in a cellular network with BS locations spatially correlated. This work introduces an inhomogeneous double thinning approach to approximate a motion-invariant PP[13] with the superposition of two inhomogeneous PPPs with the appropriate spatial correlation, which provides equivalent performance and simple simulations. Notice that inhomogeneous PPPs inherit all the main properties of homogeneous PPPs that make them mathematically tractable, but they are non-stationary and need the definition of a distance-dependent intensity function; thus, the performance of a randomly chosen user depends on its actual location. Finally, authors in [193] propose two useful distance-dependent intensity functions to create inhomogeneity based on empirically observations in practical cellular networks.

2.4.4 Rate control as another feature of the SIR meta distribution

As stated in Section 1.3, communication among MTDs can be handled through different network technologies, e.g., LoRa and Sigfox. However, these technologies suffer from some fundamental limitations, e.g., they operate over unlicensed frequency bands, making the communication links unreliable and susceptible to severe interference. Therefore, it is challenging to support applications such as monitoring systems and V2V wireless coordination that require a high degree of reliability. Moreover, network designers should consider the intrinsic trade-offs among the data rate, reliability and network lifetime arising in some applications. For instance, in precision agriculture, it is important to prolong the network lifetime and improve reliability as much as possible, while data rate requirements are less demanding.

Authors in [194] envision the importance of suitable rate control strategies to provide reliability for new services and applications in future cellular systems, and devise NOMA rate control mechanisms to increase the number of served users. Thus, implementing

[13] A PP can be invariant under translations (i.e., is stationary) and/or invariant under rotations around the origin (i.e., is isotropic) [145]. This means that under both operations the distribution of the original PP does not change.

algorithms that allow a transmitter to decide on its rate such that each link in the network achieves a certain success probability is extremely important. The idea is then to find the target SIR threshold for each link such that the conditional success probability in (11) is equal to the desired reliability $1-\epsilon$. This approach guarantees that all MTDs meet their reliability requirements. Notice that due to the nodes' random position, each link experiences different levels of interference and fading; therefore, the optimal SIR threshold, denoted as $\tilde{\theta}$, is different for each link and can be considered a random variable. Moreover, rate adaptation implies packet fragmentation to fit the time slot, which imposes a sensitive trade-off between latency and reliability [195].

For an ergodic PP, the SIR MD yields the distribution of the per-link reliability for a target SIR. Besides, authors in [196] reveal that calculating the MD as a function of SIR threshold, using any of the approaches presented in Section 2.4.2, is equivalent to compute the SIR threshold distribution such that each link is guaranteed a target reliability. In other words, for a fixed SIR threshold $\tilde{\theta} = \theta$, $\bar{F}_{P_s}(\theta, x)$ is the per-link reliability distribution, while for a fixed reliability value $x = 1-\epsilon$, $\bar{F}_{P_s}(\tilde{\theta}, 1-\epsilon)$ is the distribution of the conditional SIR threshold. Following this methodology, authors in [197] propose a distributed rate control mechanism where the transmitter only knows the distance from its receiver to the nearest interferer and the fading statistics. Based on this local information, a semi-heuristic approach is devised to obtain the distribution of $\tilde{\theta}$ corresponding to the total interference power. Surprisingly, the random SIR threshold corresponding to the total interference power is just a scaled version of that corresponding to the nearest-interferer power. Finally, authors in [198] use the MD concept to analyze the per-link rate control for open tiers (users can connect to an arbitrary tier) and closed tiers (users can only communicate inside a single tier) in heterogeneous and hybrid cellular networks. The term hybrid refers to direct communications using any of the D2D, M2M or V2V technologies.

2.4.5 Related works

In [199] and more recently in [200], authors focus on the MD of the SINR ratio and rate in HCNs with joint resource partitioning (disjoint frequency bands are allocated among tiers) and offloading[14], where users are associated with each tier with a biased average received power. Results provide important insights into the impacts of heterogeneity, resource coordination and user association. Authors in [170] study the effects of the offloading biases on the entire network and each tier in terms of the first moment and variance of $P_s(\theta)$. Using the beta distribution approximation to the MD, it is shown that the coverage performance of the existing tiers benefits from offloading users to a new tier, while the performance of the latter drops below the average of the whole network. Finally, in [201], the MD is used to study a spatiotemporal cooperation strategy to mitigate the inter-cell interference and enhance the cell-edge coverage for HCNs.

To cope with the massive access imposed by mMTC, radio access technologies such as NOMA have been lately considered. The performance analysis of this technology using the MD has been a topic of interest in recent years. For instance, authors in [116] use the MD to optimize the power allocations for downlink NOMA users and extend the

[14]Offloading in this context means to drive users to small cells using an appropriate spectrum allocation to lighten the data traffic of macro cells.

optimization problem by incorporating constraints on the mean local delays for each user. Meanwhile, the MD of the coverage probability in downlink NOMA networks is studied in [202] for two schemes, namely, everywhere in the network, where user equipments are distributed uniformly and independently in each Voronoi cell, and cell-center, where user equipments are distributed uniformly and independently in a disk around the BS. In [203], a novel user ranking technique is proposed such that the users from the cell center and cell edge regions are paired for the non-orthogonal transmission. The MD is used to provide information over the disparity in the link qualities of ranked users across the network, considering not only path-losses and fading gains but also the correlation in the inter-cell interference powers. Recently, authors in [204] show that the MD can capture the statistics of the secrecy rate in downlink NOMA systems with randomly located eavesdroppers[15].

Additionally, LPWAN technologies such as LoRaWAN constitute a connectivity solution for mMTC. To reduce energy consumption, a device in a LoRaWAN network needs to adjust its transmit power according to the distance from its tagged gateway. Authors in [206] use the MD of the SIR concept to show how fractional power control influences the coverage probability in the uplink. This is illustrated by considering the variance of the conditional coverage probability, which is lower when devices perform power control, resulting in better fairness among individual links.

In this thesis, we perform a SG-based analysis of mMTC scenarios with QoS requirements using the SIR MD tool. To gain more insights on the suitability of the adopted approach, a comparison with the analysis based on the standard success probability is also carried out.

[15]Secrecy capacity refers to the maximum transmission rate at which the eavesdropper is unable to decode any information [205].

3 A META DISTRIBUTION-BASED APPROACH FOR MMTC WITH AGGREGATION AND SCHEDULING

We presented in Section 2.1 and Section 2.2 the benefits of using data aggregation and resource scheduling, respectively. This chapter, combines the aforementioned techniques and exploits the MD concept introduced in Section 2.4 to fully characterize the uplink traffic performance in a Poisson network with cluster-based data aggregation. We present the system model and provide analytical and simulation-based performance evaluation for two scheduling mechanisms, namely RRS and CRS. Moreover, we show that the standard success probability falls short of providing Qos guarantees when targeting stringent communication errors.

3.1 System model

We investigate the uplink communication in a large-scale single-tire cellular network overlapped with aggregator nodes distributed according to an independent and homogeneous PPP, represented by Φ_p, with intensity λ_p (expected number of aggregators per area unit). Since Φ_p is a stationary process, as stated in Section 2.3, the performance analysis does not depend on each aggregator's particular location. Thus, we consider a "typical" aggregator located at the origin, which experiences interference generated by non-intended transmitters in the network.

Figure 8 shows the system model under consideration. Notice that for illustration purposes, Figure 8 also includes the MTD associated with the typical aggregator; however, since we analyze only the uplink transmission, Monte Carlo simulations do not require to draw any point in this position. Assuming that the MTDs have low mobility, we ignore complex association protocols between MTDs and aggregators (e.g., nearest-neighbor rule [207,208] and max-SIR association [209]); thus, we can model their locations as an MCP, where the aggregators form the parent PP [77]. Notice that traffic generated from low-mobility or static devices (except for V2V) is one of the MTC characteristics, in contrast to highly nomadic smartphones.

The MCP can be defined as

$$\Psi \triangleq \bigcup_{\mathbf{v}\in\Phi_p} \mathbf{v} + \mathcal{B}^{\mathbf{v}}, \tag{22}$$

where $\mathcal{B}^{\mathbf{v}}$ denotes the offspring PP, and each point $\mathbf{b} \in \mathcal{B}^{\mathbf{v}}$ is independent and identical distributed around the cluster center $\mathbf{v} \in \Phi_p$ with distance distribution $f_{R_d}(r_d) = \frac{2r_d}{R_D^2}$, where R_D is the radius of the clusters formed by the aggregators and its corresponding MTDs [137]. Since the radius of the disks is fixed in the MCP, it might be the case that a particular MTD falls within several aggregators' coverage areas as shown in Figure 8; however, each MTD is associated with a single aggregator. Notice also that some interferers fall closer to the typical aggregator than its corresponding MTD.

Consider that at any instant, the MTDs across the entire network transmit information to their serving aggregators through the same set $\mathcal{N}$ of N orthogonal channels ($N = |\mathcal{N}|$). Each aggregator can accommodate only one MTD per channel, out of K requesting service within its coverage area. Note that K is a Poisson distributed random variable with mean m, i.e., $K \sim \text{Poiss}(m)$. Thus, the only contribution to the interference comes from the MTDs in other aggregators' serving zones using the same channel (inter-cluster

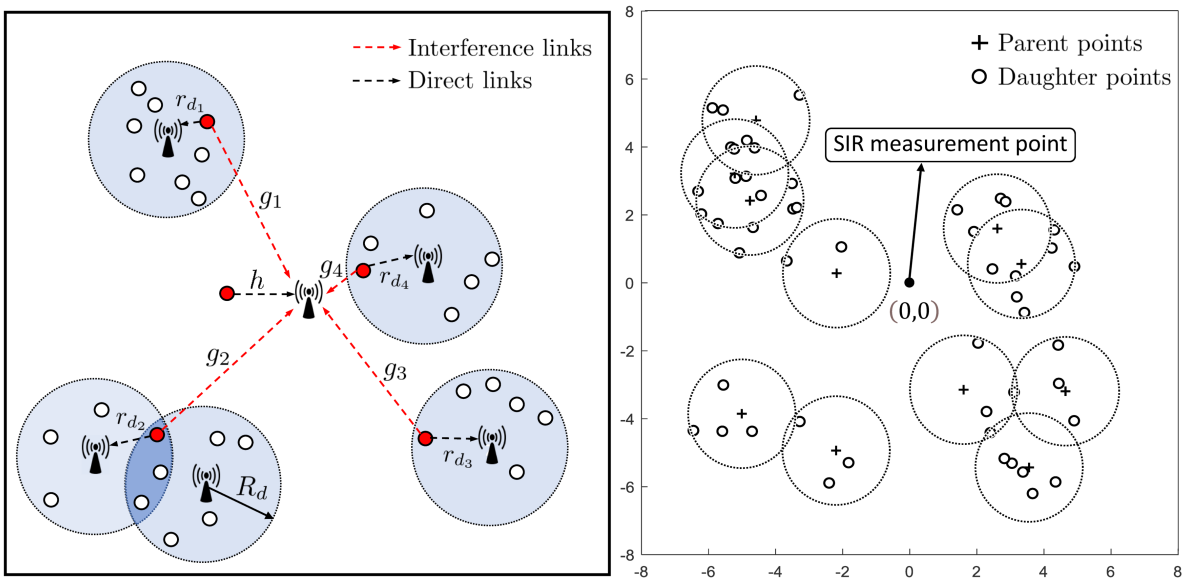

Figure 8. System Model. Illustration of direct and interference (with respect to the typical aggregator) links (left), and an MCP realization (right).

interference). Notice that each MTD transmits whenever it has new information to send, and its corresponding aggregator has allocated resources for transmission conforming two scheduling schemes described in the following sections.

3.1.1 Average channel occupation probability

The probability that any MTD within any cluster generates interference, or equivalently, the average channel occupation probability is defined as [77]

$$\begin{aligned} P_0 &= \mathbb{E}_K\left[\frac{\min(K,N)}{N}\right] \\ &= \sum_{k=0}^{N}\frac{k}{N}\frac{m^k e^{-m}}{k!} + \sum_{k=N+1}^{\infty}\frac{m^k e^{-m}}{k!} \\ &= 1 - \frac{\Gamma[1+N,m]}{N!} + \frac{m\Gamma[1+N,m] - e^{-m}m^{N+1}}{(N-1)!N^2}. \end{aligned} \tag{23}$$

Notice that P_0 is independent of the aggregators' density and the scheduling scheme performed at the aggregator since it only depends on N and m. Figure 9 shows that P_0 decreases as the number of channels available at the aggregators increases. This improves the performance since the typical link experiences less interference compared to the case where certain channel is occupied with high probability. Interestingly, for $m < N$, P_0 shows a linear dependency with m with slope $1/N$; thus, $P_0 = m/N$. Contrary, when the average number of MTDS exceeds the available resources, a particular MTD may not be assigned a channel due to the scarce resources and $P_0 = 1$. In this case, it is critical

to allocate the limited channels efficiently according to any metric that guarantees QoS, e.g., channel state condition and transmission delay.

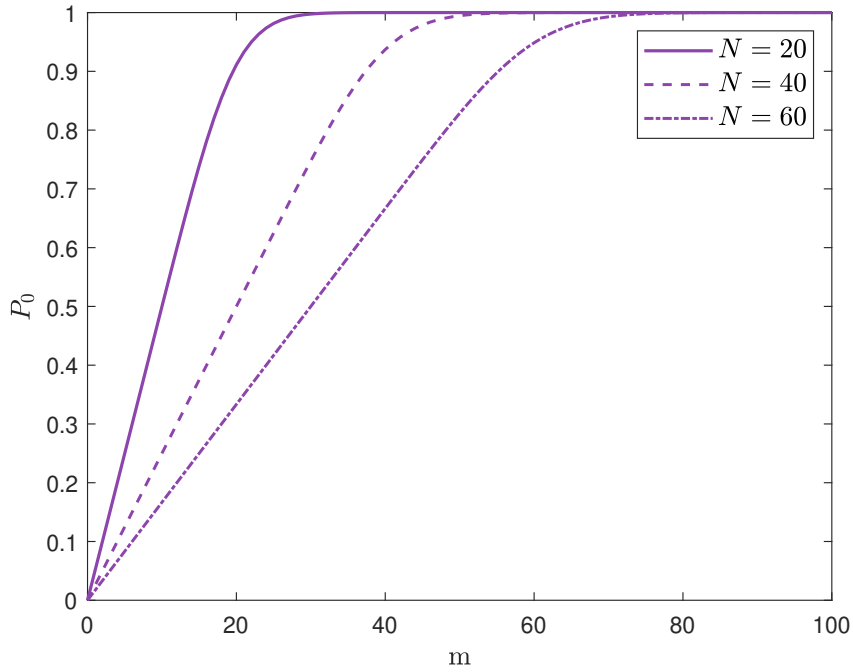

Figure 9. Average channel occupation probability versus average number of MTDs per aggregator.

3.1.2 Interfering process as a PPP

Notice that P_0 is also independent among clusters; thus, it defines an independent thinning operation and we can model the interference field observed from the typical link as a homogeneous PPP denoted as Φ_I with density $\lambda_I = P_0\lambda_p$. This statement can be properly understood by noticing that the resulting aggregators PP after selecting all the MTDs aggregators pairs communicating over the same channel is a PPP (independent thinning operation on a PPP). Moreover, each MTDs' coordinate is a random translation of that of their corresponding associated aggregators. Thus, according to the displacement theorem [114], which loosely states that the random independent displacement of points of a PPP on the same underlying space forms another PPP, we can conclude that Φ_I is a PPP as well.

For the sake of completeness, we use one of the methods introduced in Section 2.3.3 to prove equivalence among PPs. We compare the contact distribution function $F_{\Phi_I}(r)$ of Φ_I with the analytical expression corresponding to an homogeneous PPP with intensity λ_I, $F_{\text{PPP}}(r) = 1 - e^{-\lambda_I \pi r}$. To make the comparison fair enough, it is important to match the first order statistic corresponding to both PPs. Authors in [210] show that for any Poisson cluster PP, $F(r)$ approaches the one of the PPP as the clusters' radius increases to infinity and keeping the average number of points per clusters the same. However, as Figure 10 reveals, the independent thinning operation performed in this

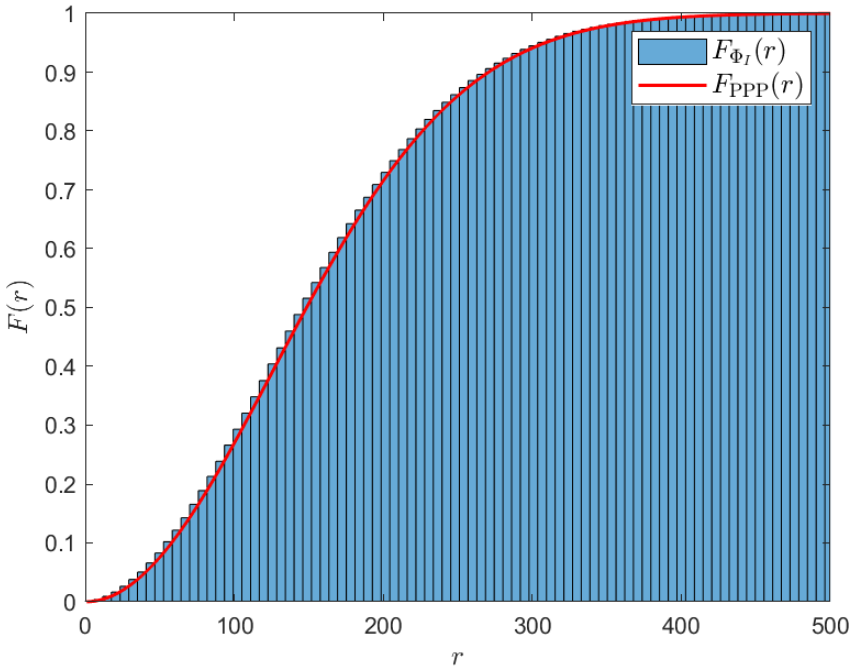

Figure 10. Contact distribution function for the thinned MCP, or equivalent, the interfering PP Φ_I. Simulation parameters: $N = 20$, $\lambda_p = 10^{-5}$, $m = 60$ and $R_D = 40$.

model's clusters allows perfect match of Φ_I to a homogeneous PPP for even small cluster's radius ($R_D = 40$). This is an important observation that permits us to use the tractable PGFL that characterize the PPP and therefore obtain "weakly closed-form"[1] solutions for the MD as it is shown in the following sections. Moreover, [211] shows that the pair correlation function of the MCP approaches that of the PPP when the average number of points per cluster tends to zero since the points are less likely to belong to the same cluster, which is the case in our model because at any time there exist at most one MTD per cluster offering interference at the typical aggregator.

Figure 11 shows the spatial similitude between a PPP generated with intensity λ_I and Φ_I. It is clear that Φ_I does not exhibit any attraction or repulsion tendency.

3.1.3 Channel and transmission model

We adopt a channel model that consists of the commonly used power-law path-loss as the large-scale propagation effect. Thus, the signal power decreases at a rate of $y^{-\alpha}$ with the propagation distance y, and $\alpha \geq 2$ is the path loss exponent. Quasi-static fading is considered as the small-scale effect, which means that the channel remains constant during a transmission block and changes independently from block to block. Notice that this statement is consistent with the assumption that MTDs stay static or have low mobility. Additionally, Rayleigh fading impairs the desired and interference links,

[1]Different from the "closed-form" term that allows only elementary functions, we use the "weakly closed-form" label for expressions involving hypergeometric, (incomplete) gamma functions, Meijer G-function and the Lambert functions (see `https://stogblog.net/category/other-points/`).

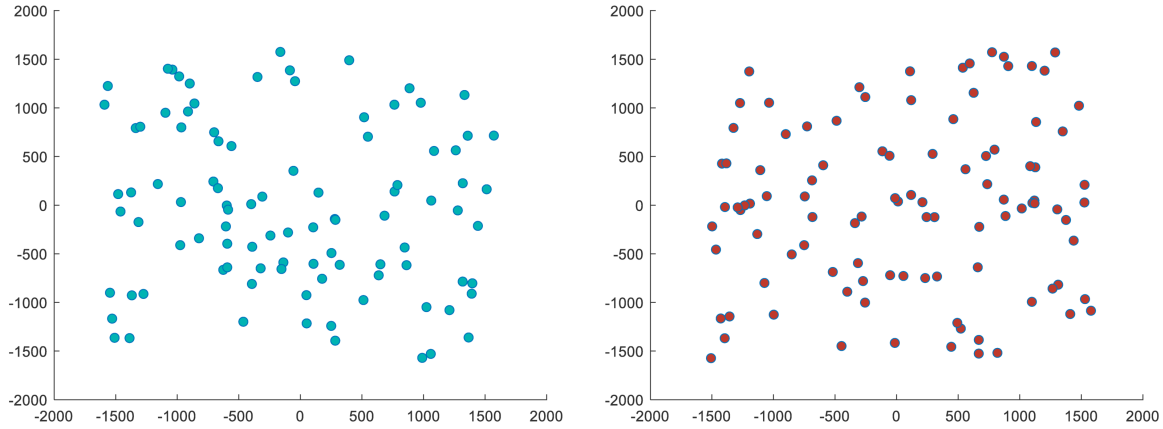

Figure 11. Interference PP Φ_I (left) and PPP with intensity λ_I (right) for $N = 20$, $\lambda_p = 10^{-5}$, $m = 60$ and $R_D = 40$.

with channel power gains—h and g, respectively—being exponential, independent and identically distributed with unit mean, i.e., h, $g \sim \text{Exp}(1)$. Notice that this assumption makes sense since the interferers' positions do not have any spatial correlation. Moreover, it allows us to examine the worst-case scenario without dominant propagation along a LoS.

All MTDs use full inversion power control. This is, each device controls its transmit power so that the average signal power received at the serving aggregator is equal to a predefined constant value ρ. In other words, each MTD transmits to its aggregator with a power equal to ρr_d^{α} to partially compensate the effect of path loss on the received signal at the aggregator [212]. This guarantees a uniform user experience while saving a critical amount of energy [101]. Since in large-scale cellular networks, the impact of the co-channel interference limits all links' performance, we consider an interference-limited scenario, and the thermal noise at the receiver side is neglected; consequently, the received SIR determines the network performance and the value of ρ is irrelevant. However, without loss of generality, the same analytical approaches provided in the next sections can also be applied to characterize performance metrics that consider the thermal noise.

3.2 Random resource scheduling (RRS)

Under RRS, each aggregator randomly assigns the channels in $\mathcal{N}$ to the MTDs. Notice that this mechanism does not need channel state information (CSI). Since the MTDs use inversion power control, the SIR experienced by the typical user is

$$\text{SIR} = \frac{h}{I} = \frac{h}{\sum_{i \in \Phi_I} g_i r_{d_i}^{\alpha} y_i^{-\alpha}}, \tag{24}$$

where I is the aggregated interference from MTDs in other clusters transmitting over the same channel, $\{y_i\}$ denotes the distance of the interfering MTDs respect the typical user, h and $\{g_i\}$ are the fading power gains on the desired and interfering links, respectively,

and $\{r_{d_i}\}$ is the distance between the MTDs and their serving aggregators. For an arbitrary but fixed realization of Ψ, the conditional success probability can be obtained from (11) as

$$\begin{aligned}
P_s(\theta) &= \mathbb{P}\left(\frac{h}{\sum\limits_{i\in\Phi_I} g_i r_{d_i}^{\alpha} y_i^{-\alpha}} \geq \theta \middle| \Psi\right) \\
&= \mathbb{E}_{g_i}\left[\mathbb{P}\left(h \geq \theta \sum_{i\in\Phi_I} g_i r_{d_i}^{\alpha} y_i^{-\alpha} \middle| g_i, \Psi\right)\right] \\
&\overset{(a)}{=} \mathbb{E}_{g_i}\left[\exp\left(-\theta \sum_{i\in\Phi_I} g_i r_{d_i}^{\alpha} y_i^{-\alpha}\right) \middle| \Psi\right] \\
&\overset{(b)}{=} \prod_{i\in\Phi_I}\left[\frac{1}{1+\theta(\frac{r_{m_i}}{y_i})^{\alpha}}\right] \\
&\overset{(c)}{=} \lim_{\eta\to\infty} \prod_{i=1}^{\eta}\left[1+\theta\left(\frac{r_{d_i}}{y_i}\right)^{\alpha}\right]^{-1} \\
&\overset{(d)}{\leq} \lim_{\eta\to\infty}\left[\frac{\sum_{i=1}^{\eta}\left[1+\theta\left(\frac{r_{d_i}}{y_i}\right)^{\alpha}\right]}{\eta}\right]^{-\eta} \\
&\overset{(e)}{=} \lim_{\eta\to\infty}\left[1+\frac{\theta}{\eta}\sum_{i=1}^{\eta}\left(\frac{r_{d_i}}{y_i}\right)^{\alpha}\right]^{-\eta} \\
&= \lim_{\eta\to\infty}\left[1+\frac{\theta}{\eta}\beta\right]^{-\eta} \\
&\overset{(f)}{\approx} e^{-\beta\theta},
\end{aligned} \tag{25}$$

where (a) comes from applying the complementary CDF of the unit mean exponential distribution of h; (b) follows from using the Laplace transform of the sum of independent and identical distributed exponential random variables $\{g_i\}$; in (c), we consider the number of interfering nodes as η, and then use the relation between the geometric and the arithmetic mean to obtain (d). Note that interchanging geometric and arithmetic means was shown to conduce to accurate performance expressions in [213] for sufficiently dense networks without aggregation. Finally, (e) comes from simple algebraic transformations; and (f) results from making

$$\beta = \sum_{i=1}^{\eta}\left(\frac{r_{d_i}}{y_i}\right)^{\alpha} \tag{26}$$

Remark 1. *Obtaining the PDF of $P_s(\theta)$ directly from (b) seems infeasible for massive network deployments; thus, in this case, we adopt approximation (25) to attain the final SIR MD analytical expression.*

With (25) in hands, we can compute the MD for this scheduling scheme by plugging it into (12). However, β is a random variable that depends on the network's geometry; thus, we need its PDF. We proceed as follows

$$\begin{aligned}
\mathcal{L}_{\beta}(s) &= \mathbb{E}_{\Phi_I, r_d}\Big[\exp\Big(-s\sum_{i\in\Phi_I}\Big(\tfrac{r_{d_i}}{y_i}\Big)^{\alpha}\Big)\Big] \\
&= \mathbb{E}_{\Phi_I}\prod_{i\in\Phi_I}\mathbb{E}_{r_d}\Big[\exp\Big(-s\Big(\tfrac{r_{d_i}}{y_i}\Big)^{\alpha}\Big)\Big] \\
&\overset{(a)}{=} \exp\Bigg(-2\pi\lambda\int_0^{\infty}\Big(1-\mathbb{E}_{r_d}\Big[\exp\Big(-s\Big(\tfrac{r_d}{y}\Big)^{\alpha}\Big)\Big]\Big)ydy\Bigg) \\
&\overset{(b)}{=} \exp\Bigg(\tfrac{-2\pi\lambda}{\alpha}\mathbb{E}_{r_d}\int_0^{\infty}\Big[1-\exp\Big(\tfrac{-sr_d^{\alpha}}{w}\Big)\Big]w^{\frac{2}{\alpha}-1}dw\Bigg) \\
&\overset{(c)}{=} \exp\Bigg(-\pi P_0\lambda_p\mathbb{E}_{r_d}\Big[\mathbb{E}_w\Big[\Big(\tfrac{w}{(sr_d)^{\alpha}}\Big)^{-\frac{2}{\alpha}}\Big)\Big]\Big]\Bigg) \\
&= \exp\Big(-\pi P_0\lambda_p\mathbb{E}_{r_d}[r_d^2]\ \mathbb{E}_w\Big[w^{\frac{2}{\alpha}}\Big]\Big) \\
&= \exp\Big(-\pi P_0\lambda_p\tfrac{R_D^2}{2}\Gamma\Big(1-\tfrac{2}{\alpha}\Big)s^{\frac{2}{\alpha}}\Big) \\
&= \exp\Big(-ts^{\frac{2}{\alpha}}\Big),
\end{aligned} \tag{27}$$

where (a) comes from applying the PGFL defined in [146], [214]; (b) follows from the substitution $y^{-\alpha} = \frac{1}{w}$; (c) is obtained using the following definition of moment of a non-negative continuous real random variable $\mathbb{E}[z^n] = \int nz^{n-1}(1-F(z))dz$, and by noticing that $\mathbb{E}_w\left(w^{\frac{2}{\alpha}}\right)$ is the expected value of an exponential random variable with unitary mean. $\Gamma(\cdot)$ is the gamma function defined in [215, Eq. (5.2.1)], which make (27) only valid for $\alpha > 2$. This is because for $\alpha < 2$, the average cumulated contribution from many distant interfererers do not decay fast enough to keep the interference power bounded. Finally, (27) is obtained by performing the substitution $t = \frac{1}{2}P_0\lambda_p\pi R_D^2\Gamma\left(1-\frac{2}{\alpha}\right)$.

Result in (27) has the form of a stretched exponential or Kohlrausch function, i.e, $e^{-ts^{2/\alpha}}$ for a certain constant t [216]. In [217, Table I], the authors provide the PDF of such random variables for different values of α. Herein, we adopt these results and set α to 4 for simplicity. Then, the PDF of β is given by [217, Table I]

$$f_{\beta}(\omega) = \frac{te^{\frac{-t^2}{4\omega}}}{2\sqrt{\pi}\omega^{\frac{3}{2}}}. \tag{28}$$

This is a Lévy distribution [218, 219], i.e., $\beta \sim \text{Levy}(0, \frac{t^2}{2})$, which belongs to the heavy-tail[2] distribution family; thus, large values of β have high occurrence probability, which can have a dramatic effect on the system average behaviour. Thus, traditional conception of average is not longer applicable since the law of large numbers does not hold. This is extremely important to consider, as Figure 12 shows, specially when the aggregator's

[2]Heavy-tailed distributions are probability distributions whose tails are not exponentially bounded; it decays polynomially (slower decline) e.g., Pareto, Log-Normal, Weibull, Log-Gamma and Burr distributions. [220] shows experimental evidences of the interference's heavy tailed nature in the context of IoT communications.

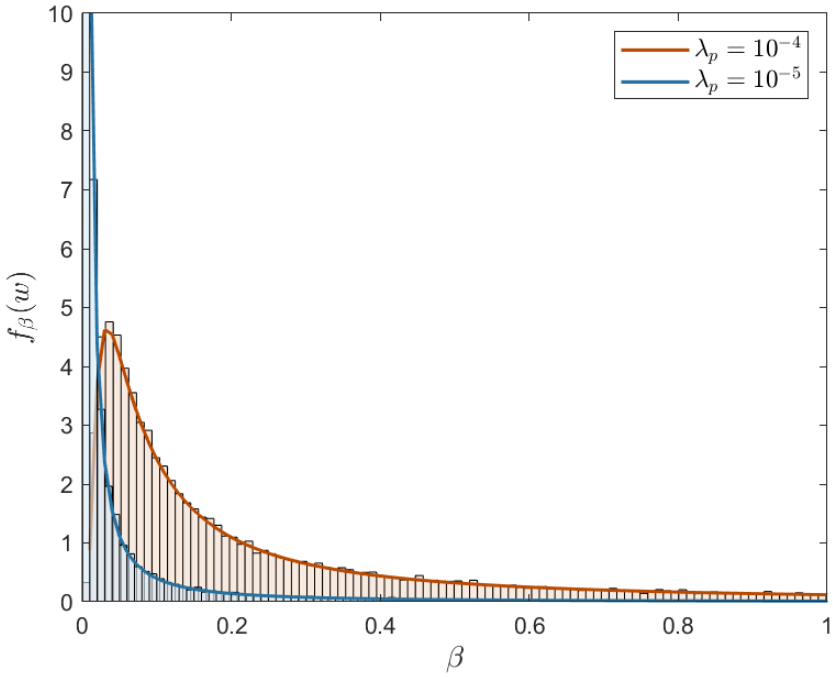

Figure 12. PDF of β (Lévy distribution) for different aggregator's intensity λ_p.

density increases and clusters fall closer to the typical point; in which case $|y_i| < |r_{d_i}|$ and the interference levels increment. Notice the tremendous importance of (28) that even for dense networks ($\lambda_p > 10^{-4}$) it perfectly reflects the tail behaviour. Moreover, as we consider a higher aggregators density, the simulation run-time increases; thus, analytical expressions that provide fast insights into the network performance are essential for network designers, particular in time constrained projects.

Combining (12), (25) and (28), we attain the SIR MD under RRS as

$$\begin{aligned}
\bar{F}(\theta, x) &= \mathbb{P}\left(e^{-\beta\theta} > x\right) \\
&= \mathbb{P}\left(\beta < \frac{-\ln x}{\theta}\right) \\
&= \int_0^{\frac{-\ln x}{\omega}} f_\beta(\omega) d\omega \\
&= \int_0^{\frac{-\ln x}{\theta}} \frac{t e^{\frac{-t^2}{4\omega}}}{2\sqrt{\pi}\omega^{\frac{3}{2}}} d\omega \ ^{(a)} \\
&= b \int_{\frac{-\theta}{\ln x}}^{\infty} u^{\frac{1}{2}-1} e^{-au} du \\
&= b a^{-\frac{1}{2}} \Gamma\left(\frac{1}{2}, -\frac{\theta a}{\ln x}\right),
\end{aligned} \tag{29}$$

where (a) comes from substituting $\frac{1}{\omega} = u$, $a = \frac{t^2}{4}$ and $b = \frac{t}{2\sqrt{\pi}}$. Notice that the same procedure to compute the SIR MD in (29) applies for any integer value of path loss exponent $\alpha > 2$. However, in these cases, the PDF of β have complicated forms that depends on multiple Bessel and hypergeometric functions; thus, the previous integration

procedure would be tedious and hard to obtain insights from the result. To cope with this issue, we also provide an upper bound to the MD by combining (12) and (25) as

$$\begin{aligned}\bar{F}(\theta, x) &= \mathbb{P}\left(e^{-\beta\theta} > x\right) \\ &= \mathbb{P}\left(\beta < \frac{-\ln x}{\theta}\right) \\ &\overset{(a)}{\leq} \min_{\xi \geq 0} e^{-\frac{\ln x}{\theta}\xi} \mathbb{E}[e^{-\xi\beta}] \\ &\overset{(b)}{=} \min_{\xi \geq 0} e^{-\left(\frac{\ln x}{\theta}\xi + t\xi^{\frac{2}{\alpha}}\right)},\end{aligned} \tag{30}$$

where (a) comes from applying Chernoff bound and (b) from realizing that the expectation in (a) can be interpreted as the Laplace transform of β, and by substituting $s = \xi$ in (27). Notice that (30) is a decreasing exponential objective function; thus, it is enough to find the minimum value of the argument that satisfy the constraint. By finding the first derivative and equate to zero, we obtain that the optimal value is

$$\xi^* = \left[-\frac{\alpha \ln x}{2t\theta}\right]^{\frac{\alpha}{2-\alpha}}. \tag{31}$$

It is easy to note that $\xi^* \geq 0$; thus it satisfies the constraint. Figure 13 shows the accuracy of Chernoff bound for RRS (30).

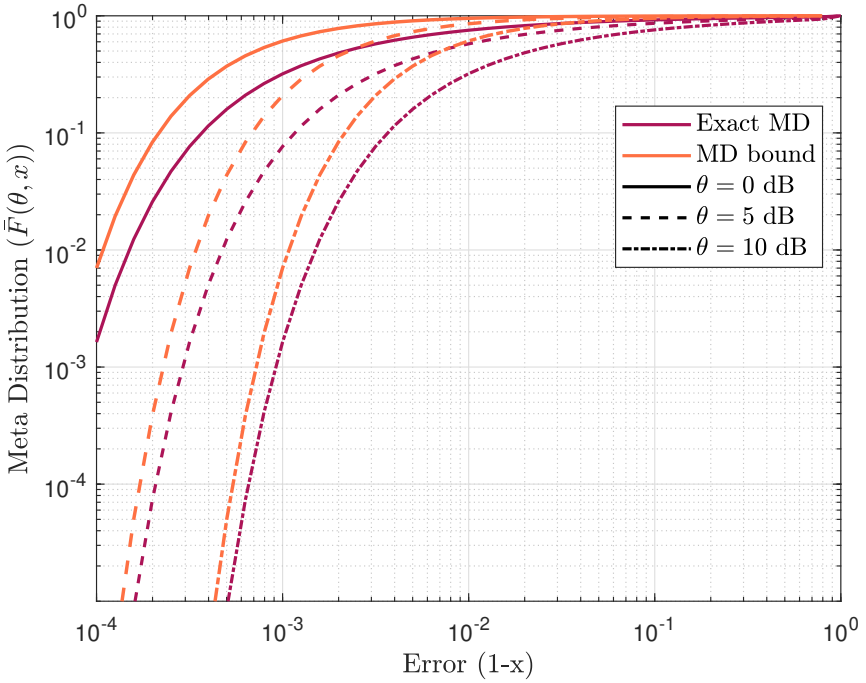

Figure 13. Exact MD (29), and the bound obtained from (30) for $\lambda_p = 10^{-5}$, $\alpha = 4$, $R_D = 40$, $N = 20$ and $m = 60$.

3.3 Channel-aware resource scheduling (CRS)

Contrary to the RRS scheme, the aggregators that implement CRS allocate the available channel resources to the MTDs with better SIR (equivalently, better channel gains). Herein, each aggregator is assumed with perfect CSI of the links of its associated MTDs. From (11), we have that the conditional success probability corresponding to the ν-th link with $h(\nu)$ channel power gain is

$$P_s(\theta) \triangleq \mathbb{P}(\text{SIR} > \theta|\Psi) = 1 - \mathbb{P}(h(\nu) < \theta I|\Psi), \tag{32}$$

where $\nu = 1, ..., N$ corresponds to the selected MTDs ordered according their SIR as $h(1) > \ldots > h(\nu) > \ldots > h(N)$. Then, the CDF of $h(\nu)$ using order statistics results is

$$F_{h(\nu)}(v) = \sum_{l=q}^{K} \binom{K}{l} [F_h(v)]^l [1 - F_h(v)]^{K-l}, \tag{33}$$

where $q = K - \nu + 1$ and $F_h(v)$ is the CDF of an exponential random variable. Then, the SIR MD under CRS is obtained as

$$\begin{aligned}
\bar{F}(\theta, x) &\overset{(a)}{=} \mathbb{P}\left(1 - \sum_{l=q}^{K} \binom{K}{l} \mathbb{E}_I \left[[1 - e^{-I\theta}]^l e^{-I\theta(K-l)} \Big| \Psi \right] > x \right) \\
&\overset{(b)}{=} \mathbb{P}\left(1 - \sum_{l=q}^{K} \sum_{r=0}^{l} \binom{K}{l} \binom{l}{r} (-1)^r \mathbb{E}_I \left[e^{-I\theta(K-l+r)} \Big| \Psi \right] > x \right) \\
&\overset{(c)}{=} \mathbb{P}\left(1 - \sum_{l=q}^{K} \sum_{r=0}^{l} \binom{K}{l} \binom{l}{r} (-1)^r \prod_{i \in \Phi_I} \frac{1}{1 + \theta_{l,r} (\frac{r_{d_i}}{y_i})^\alpha} > x \right),
\end{aligned} \tag{34}$$

where (a) comes from combining (12), (32) and (33); (b) is obtained by using the binomial expansion $(1+z)^l = \sum_{r=0}^{l} \binom{l}{r} z^r$; and (c) follows from considering the expectation in (b) as the interference Laplace transform conditioned on the PP, and by making $\theta_{l,r} = \theta(K - l + r)$.

Figure 14 shows the MD (34) for different values of ν. Herein, we analyze the worst-case performance, which is when $\nu = N$. This is, we consider the link with the smallest channel coefficient among all the links with access granted by the aggregator. Thus, by setting $q = K - N + 1$ in (34), we avoid averaging over all possibilities of ν, reducing complexity while keeping the per-link performance guarantee concept. Notice that considering all choices of ν would lead to an average result, which contradicts the MD concept. Moreover, (34) allows a semi-analytical computation of the MD that depends only on the interfering nodes' position inside the clusters and with respect to the typical link. Therefore, it is unnecessary to model either the channel fading or the scheduling process, which reduces the computation time significantly.

3.4 Performance evaluation and numerical results

This section presents numerical results to analyze the per-link performance in an mMTC setup with data aggregation under RRS and CRS. The aggregators are deployed in a

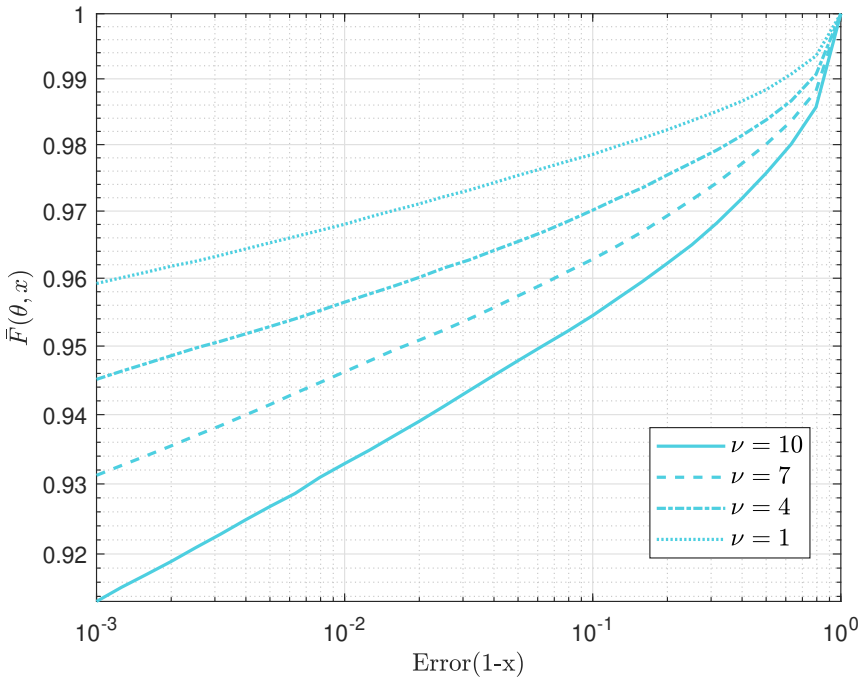

Figure 14. MD of the SIR (semi-analytical (34)) according to different ordered channels (ν). Simulation parameters: $\lambda_p = 10^{-5}$, $\alpha = 4$, $R_D = 40$, $\theta = 0$ dB, $N = 10$ and $m = 20$.

disk of radius 3 km with density $\lambda_p = 3 \times 10^{-6}$ aggregators/m^2, which guarantees 100 aggregators deployed on average in the area while eliminating the impact of the border effect in the simulation. As it was stated in Section 2.3.3, the edge effect can be neglected as the simulation window is selected large enough. It was selected $N = 20$, $m = 60$, and $R_D = 40$ m to produce visualization errors in the order of 10^{-2}. Monte Carlo based results are obtained with 10^5 samples and are included in the figures with markers to validate our analytical (for RRS) and semi-analytical (for CRS) expressions, which are represented with lines.

Figure 15 shows the efficacy of the SIR MD for describing the system per-link performance. One can realize that the traditional p_s does not guarantee QoS for any node in the network, which is even more remarkable when RRS is enabled in the aggregation phase. This is because the channels are assigned to links that communicate with high error probability. In contrast, having the MD in hand allows effective distribution of these resources as the exact fraction of links communicating with a target reliability is known in advance. Moreover, aggregators implementing CRS admit a higher percentage of links achieving a target reliability in the resources-constrained communication system.

Figure 16 permits a more rigorous analysis of the fraction of links that achieve certain reliability given the SIR threshold θ. For example, the marked point shows that the transmission rate should be set no greater than $\log_2(1 + 10^{-5/10}) = 0.396$ bits per channel use (bpcu) to guarantee nearly 86% of the links achieving at least 99.9% success probability when operating with RRS. One may notice that nearly the same fraction of devices can transmit with the same rate under both scheduling schemes, but with reliability improved from 0.9 when using RRS to 0.999 under CRS. If simplicity is desired in the network, RRS is the solution, but only a small percentage of devices achieve high

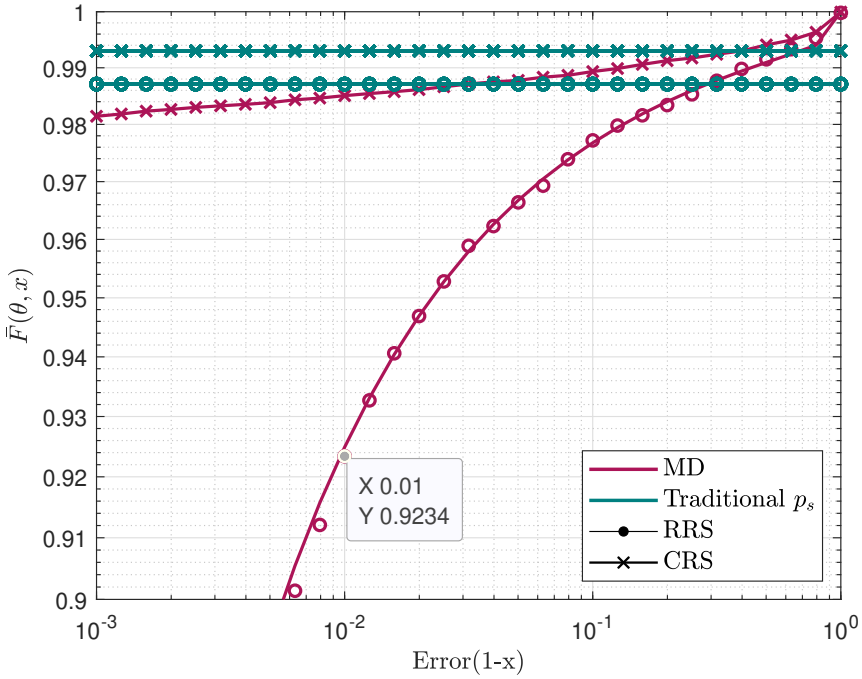

Figure 15. MD and the traditional success probability (p_s) for $\alpha = 4$ and $\theta = 0$ dB. The marked point can be interpreted as approximately 92% of the users can communicate with 0.01 probability of error.

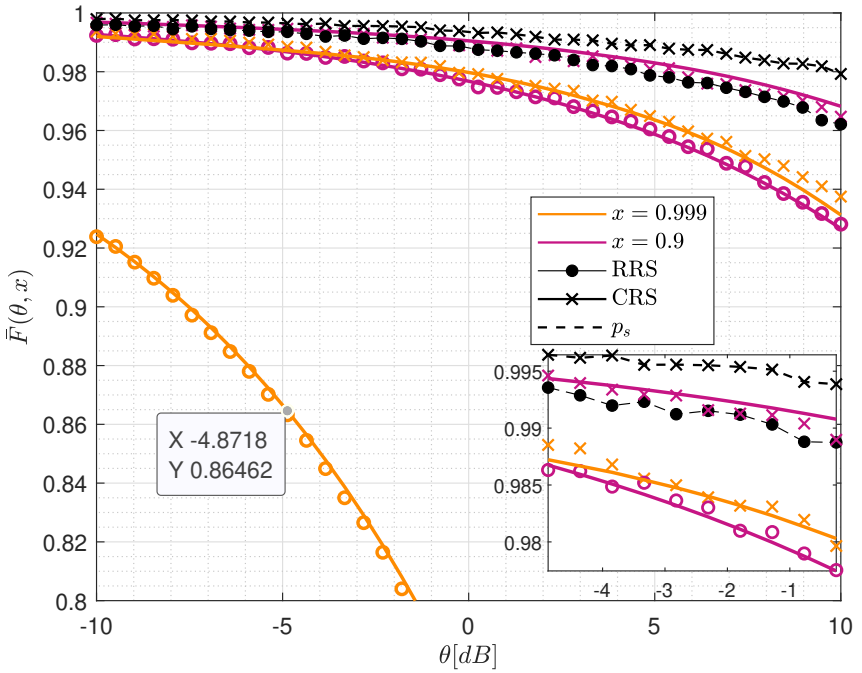

Figure 16. MD and traditional success probability (p_s) as a function of θ for different values of reliability (x).

reliability. However, if a larger number of devices need to communicate, CRS seems to be the best option to provide them the required reliability.

Figure 17 visualizes the trade-off between the transmit rate and m. In general, the transmit rate has to decrease when the number of MTDs requesting transmission

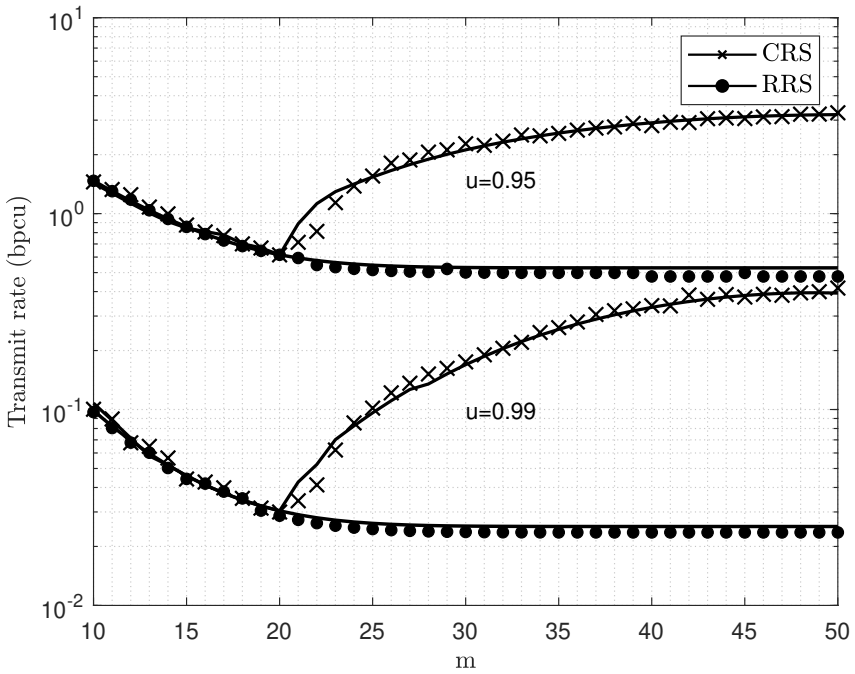

Figure 17. Transmit rate versus average number of MTDs per aggregator for $\bar{F}(\theta, x) = u = 0.99, 0.95$ and $x = 99\%$ of reliability.

approaches the available resources. However, when this value exceeds N, the probability of selecting a better channel under CRS increases, and the transmit rate can improve. In contrast, under RRS the rate cannot exceed a constant value. Notice that the percentage of devices communicating with the target reliability must remain the same in both cases.

Figure 18 shows an important trade-off that network designers need to consider. This

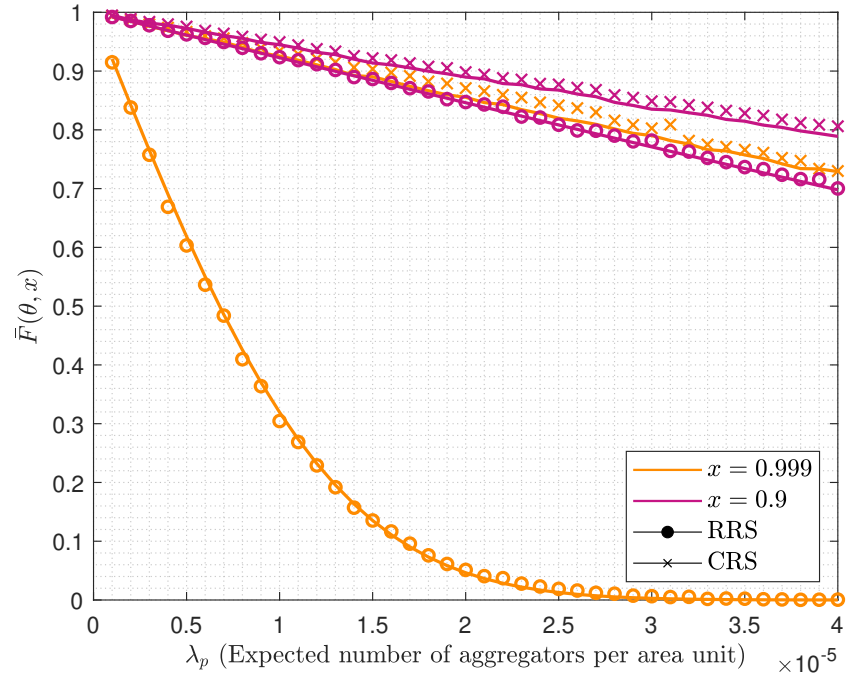

Figure 18. Meta distribution as a function of λ_p for $\alpha = 4$, $\theta = 0$ dB and $x = 0.999, 0.9$.

is, the aggregators' density cannot increase loosely; otherwise, only a small fraction of MTDs would communicate with the target reliability. Notice that this is due to the static cluster-based hierarchy where increasing λ_p implies also increasing the number of MTDs and therefore the interference. On the other hand, it is clear that as λ_p approaches 0, the percentage of MTDs achieving the target reliability increases, but obviously the benefits from aggregation also disappear. Notice that, in general, the density of served MTDs increases with λ_p. However, under RRS, almost no transmission satisfies 99% of reliability. Moreover, based on these figure results, one can determine the density of MTDs that allows reaching an SIR θ with reliability x, which is given by $\lambda_p P_0 \bar{F}(\theta, x)$.

4 CONCLUSIONS

In this thesis, we exposed the main challenges arising from MTC compared to traditional HTC. Moreover, the most promising technologies to support mMTC in the context of IoT were described. Important SG aspects to model dense network deployments using PPs were also presented. We analyzed the MD of the SIR to provide a more fine-grained description of the per-link performance under RRS and CRS scheduling schemes compared to the analyses derived from the traditional success probability. Our results showed that RRS performs extremely poor in terms of per-link reliability compared to CRS when a limited amount of resources can be scheduled among the MTDs. This is, RRS guarantees the same per-link reliability performance as CRS but for a smaller number of communication links. This difference is more significant when targeting stringent reliability performance. We also revealed that CRS allows to increase the transmission rate when the number of MTDs exceeds the available resources. Finally, we showed that the percentage of successful transmissions meeting a target reliability decreases as the aggregators density increases.

This work can be extended as follows:

- Exploring analytical approaches to characterize the MD under CRS.
- Implementing more sophisticated scheduling policies that consider others QoS requirements suitable for delay-sensitive IoT applications. A spatio-temporal model based on the MD and queuing theory to account for IoT devices' spatial and temporal attributes could be an interesting approach.
- Implement an algorithm that ensures efficient power and rate control in these challenging scenarios.
- In this thesis, we assumed perfect CSI at the aggregators. However, an interesting extension would also consider imperfect CSI and non-coherent decoding schemes.

5 REFERENCES

[1] Arshad Q.K.U.D., Kashif A.U. & Quershi I.M. (2019) A review on the evolution of cellular technologies. In: 16th International Bhurban Conference on Applied Sciences and Technology (IBCAST), IEEE, pp. 989–993.

[2] Mircea M., Stoica M. & Ghilic-Micu B. (2017) Using cloud computing to address challenges raised by the Internet of Things. In: Connected Environments for the Internet of Things, Springer, pp. 63–82.

[3] Corcoran P. (2015) The Internet of Things: Why now, and what's next? IEEE consumer electronics magazine 5, pp. 63–68.

[4] Mahmood N.H., Böcker S., Munari A., Clazzer F., Moerman I., Mikhaylov K., López O.A., Park O., Mercier E., Bartz H., Jüntti R., Pragada R.V., Ma Y., Annanperä E., Wietfeld C., Andraud M., Liva G., Chen Y., Garro E., Burkhardt F., Alves H., Liu C., Sadi Y., Doré J., Kim E., Shin J., Park G.Y., Kim S., Yoon C., Anwar K. & Seppänen P. (2020) White paper on critical and massive machine type communication towards 6G. ArXiv abs/2004.14146.

[5] Latva-aho M. & Leppänen K. (2019) Key drivers and research challenges for 6G ubiquitous wireless intelligence.

[6] Mocrii D., Chen Y. & Musilek P. (2018) IoT-based smart homes: A review of system architecture, software, communications, privacy and security. Internet of Things 1, pp. 81–98.

[7] Dian F.J., Vahidnia R. & Rahmati A. (2020) Wearables and the Internet of Things (IoT), applications, opportunities, and challenges: A survey. IEEE Access 8, pp. 69200–69211.

[8] Davoody-Beni Z., Sheini-Shahvand N., Shahinzadeh H., Moazzami M., Shaneh M. & Gharehpetian G.B. (2019) Application of IoT in smart grid: Challenges and solutions. In: 5th Iranian Conference on Signal Processing and Intelligent Systems (ICSPIS), IEEE, pp. 1–8.

[9] Mahmood Z. (2020) Connected Vehicles in the Internet of Things. Springer.

[10] Farooq M.S., Riaz S., Abid A., Abid K. & Naeem M.A. (2019) A survey on the role of IoT in agriculture for the implementation of smart farming. IEEE Access 7, pp. 156237–156271.

[11] Akpakwu G.A., Silva B.J., Hancke G.P. & Abu-Mahfouz A.M. (2017) A survey on 5G networks for the Internet of Things: Communication technologies and challenges. IEEE access 6, pp. 3619–3647.

[12] Yin X., Liu J., Cheng X., Zeng B. & Xiong X. (2020) A low-complexity design for the terminal device of the urban IoT-oriented heterogeneous network with ultra-high-speed OFDM processing. Sustainable Cities and Society 61, p. 102323.

[13] Alioto M. (2017) Enabling the Internet of Things: From Integrated Circuits to Integrated Systems. Springer.

[14] Henkel J., Pagani S., Amrouch H., Bauer L. & Samie F. (2017) Ultra-low power and dependability for IoT devices. In: Design, Automation & Test in Europe Conference & Exhibition, p. 954959.

[15] Eltresy N.A., Dardeer O.M., Al-Habal A., Elhariri E., Abotaleb A.M., Elsheakh D.N., Khattab A., Taie S.A., Mostafa H., Elsadek H.A. et al. (2020) Smart home IoT system by using RF energy harvesting. Journal of Sensors 2020.

[16] Abdul-Qawy A.S.H., Almurisi N.M.S. & Tadisetty S. (2020) Classification of energy saving techniques for IoT-based heterogeneous wireless nodes. Procedia Computer Science 171, pp. 2590–2599.

[17] Adegbija T., Rogacs A., Patel C. & Gordon-Ross A. (2017) Microprocessor optimizations for the Internet of Things: A survey. IEEE Transactions on Computer-Aided Design of Integrated Circuits and Systems 37, pp. 7–20.

[18] Maheepala M., Joordens M.A. & Kouzani A.Z. (2020) Low power processors and image sensors for vision-based IoT devices: A review. IEEE Sensors Journal 21, pp. 1172–1186.

[19] Kozłowski A. & Sosnowski J. (2019) Energy efficiency trade-off between duty-cycling and wake-up radio techniques in IoT networks. Wireless Personal Communications 107, pp. 1951–1971.

[20] Shrouf F., Ordieres J. & Miragliotta G. (2014) Smart factories in industry 4.0: A review of the concept and of energy management approached in production based on the Internet of Things paradigm. In: 2014 IEEE international conference on industrial engineering and engineering management, IEEE, pp. 697–701.

[21] Molaei F., Rahimi E., Siavoshi H., Afrouz S.G. & Tenorio V. (2020) A comprehensive review on Internet of Things (IoT) and its implications in the mining industry. American Journal of Engineering and Applied Sciences 13, pp. 499–515.

[22] Mohammadi M., Al-Fuqaha A., Sorour S. & Guizani M. (2018) Deep learning for IoT big data and streaming analytics: A survey. IEEE Communications Surveys & Tutorials 20, pp. 2923–2960.

[23] Mahdavinejad M.S., Rezvan M., Barekatain M., Adibi P., Barnaghi P. & Sheth A.P. (2018) Machine learning for Internet of Things data analysis: A survey. Digital Communications and Networks 4, pp. 161–175.

[24] Nalbandian S. (2015) A survey on Internet of Things: Applications and challenges. In: International Congress on Technology, Communication and Knowledge (ICTCK), IEEE, pp. 165–169.

[25] Queralta J.P., Gia T.N., Zou Z., Tenhunen H. & Westerlund T. (2019) Comparative study of LPWAN technologies on unlicensed bands for M2M communication in the IoT: Beyond LoRa and LoRaWAN. Procedia Computer Science 155, pp. 343–350.

[26] Qadir Q.M., Rashid T.A., Al-Salihi N.K., Ismael B., Kist A.A. & Zhang Z. (2018) Low power wide area networks: A survey of enabling technologies, applications and interoperability needs. IEEE Access 6, pp. 77454–77473.

[27] Metongnon L. & Sadre R. (2018) Fast and efficient probing of heterogeneous IoT networks. International Journal of Network Management 28, p. e1997.

[28] Al-Qaseemi S.A., Almulhim H.A., Almulhim M.F. & Chaudhry S.R. (2016) IoT architecture challenges and issues: Lack of standardization. In: Future technologies conference (FTC), IEEE, pp. 731–738.

[29] Centenaro M., Vangelista L., Zanella A. & Zorzi M. (2016) Long-range communications in unlicensed bands: The rising stars in the IoT and smart city scenarios. IEEE Wireless Communications 23, pp. 60–67.

[30] Chen H., Abbas R., Cheng P., Shirvanimoghaddam M., Hardjawana W., Bao W., Li Y. & Vucetic B. (2018) Ultra-reliable low latency cellular networks: Use cases, challenges and approaches. IEEE Communications Magazine 56, pp. 119–125.

[31] Karie N.M., Sahri N.M. & Haskell-Dowland P. (2020) IoT threat detection advances, challenges and future directions. In: 2020 Workshop on Emerging Technologies for Security in IoT (ETSecIoT), IEEE, pp. 22–29.

[32] Tehrani M.N., Uysal M. & Yanikomeroglu H. (2014) Device-to-device communication in 5G cellular networks: challenges, solutions, and future directions. IEEE Communications Magazine 52, pp. 86–92.

[33] Kar U.N. & Sanyal D.K. (2018) An overview of device-to-device communication in cellular networks. ICT express 4, pp. 203–208.

[34] Jameel F., Hamid Z., Jabeen F., Zeadally S. & Javed M.A. (2018) A survey of device-to-device communications: Research issues and challenges. IEEE Communications Surveys & Tutorials 20, pp. 2133–2168.

[35] Björnson E., Hoydis J. & Sanguinetti L. (2017) Massive MIMO networks: Spectral, energy, and hardware efficiency. Foundations and Trends in Signal Processing 11, pp. 154–655.

[36] Marzetta T.L. (2010) Noncooperative cellular wireless with unlimited numbers of base station antennas. IEEE transactions on wireless communications 9, pp. 3590–3600.

[37] Björnson E., Sanguinetti L., Wymeersch H., Hoydis J. & Marzetta T.L. (2019) Massive MIMO is a reality—what is next?: Five promising research directions for antenna arrays. Digital Signal Processing 94, pp. 3–20.

[38] Ali E., Ismail M., Nordin R. & Abdulah N.F. (2017) Beamforming techniques for massive MIMO systems in 5G: overview, classification, and trends for future research. Frontiers of Information Technology & Electronic Engineering 18, pp. 753–772.

[39] Chataut R. & Akl R. (2020) Massive MIMO systems for 5G and beyond networks—overview, recent trends, challenges, and future research direction. Sensors 20, p. 2753.

[40] Saunders S.R., Aragï A. et al. (2007) Antennas and propagation for wireless communication systems. John Wiley & Sons.

[41] Qin Q., Gui L., Cheng P. & Gong B. (2018) Time-varying channel estimation for millimeter wave multiuser MIMO systems. IEEE Transactions on Vehicular Technology 67, pp. 9435–9448.

[42] Alrabeiah M. & Alkhateeb A. (2020) Deep learning for mmWave beam and blockage prediction using sub-6GHz channels. IEEE Transactions on Communications 68, pp. 5504–5518.

[43] Kamel M., Hamouda W. & Youssef A. (2016) Ultra-dense networks: A survey. IEEE Communications Surveys & Tutorials 18, pp. 2522–2545.

[44] Stefanatos S. & Alexiou A. (2014) Access point density and bandwidth partitioning in ultra dense wireless networks. IEEE transactions on communications 62, pp. 3376–3384.

[45] Zamani A., Kämmer R., Hu Y. & Schmeink A. (2020) Optimization of unmanned aerial vehicle augmented ultra-dense networks. EURASIP Journal on Wireless Communications and Networking 2020, pp. 1–17.

[46] Duong T.Q., Chu X. & Suraweera H.A. (2019) Ultra-dense networks for 5G and beyond: modelling, analysis, and applications. John Wiley & Sons.

[47] Song X., Geng Y., Meng X., Liu J., Lei W. & Wen Y. (2017) Cache-enabled device to device networks with contention-based multimedia delivery. IEEE Access 5, pp. 3228–3239.

[48] Adedoyin M.A. & Falowo O.E. (2020) Combination of ultra-dense networks and other 5G enabling technologies: a survey. IEEE Access 8, pp. 22893–22932.

[49] Kim H. (2020) Design and Optimization for 5G Wireless Communications. John Wiley & Sons.

[50] Popovski P., Trillingsgaard K.F., Simeone O. & Durisi G. (2018) 5G wireless network slicing for eMBB, URLLC, and mMTC: A communication-theoretic view. IEEE Access 6, pp. 55765–55779.

[51] Bennis M., Debbah M. & Poor H.V. (2018) Ultrareliable and low-latency wireless communication: Tail, risk, and scale. Proceedings of the IEEE 106, pp. 1834–1853.

[52] Popovski P., Stefanović Č., Nielsen J.J., De Carvalho E., Angjelichinoski M., Trillingsgaard K.F. & Bana A.S. (2019) Wireless access in ultra-reliable low-latency communication (URLLC). IEEE Transactions on Communications 67, pp. 5783–5801.

[53] Alcaraz López O.L., Mahmood N.H. & Alves H. (2020) Enabling URLLC for low-cost IoT devices via diversity combining schemes. In: 2020 IEEE International Conference on Communications Workshops (ICC Workshops), pp. 1–6.

[54] Schulz P., Matthe M., Klessig H., Simsek M., Fettweis G., Ansari J., Ashraf S.A., Almeroth B., Voigt J., Riedel I. et al. (2017) Latency critical IoT applications in 5G: Perspective on the design of radio interface and network architecture. IEEE Communications Magazine 55, pp. 70–78.

[55] Ji H., Park S., Yeo J., Kim Y., Lee J. & Shim B. (2018) Ultra-reliable and low-latency communications in 5G downlink: Physical layer aspects. IEEE Wireless Communications 25, pp. 124–130.

[56] Bockelmann C., Pratas N.K., Wunder G., Saur S., Navarro M., Gregoratti D., Vivier G., De Carvalho E., Ji Y., Stefanovic C. et al. (2018) Towards massive connectivity support for scalable mMTC communications in 5G networks. IEEE access 6, pp. 28969–28992.

[57] Bockelmann C., Pratas N., Nikopour H., Au K., Svensson T., Stefanovic C., Popovski P. & Dekorsy A. (2016) Massive machine-type communications in 5G: Physical and MAC-layer solutions. IEEE Communications Magazine 54, pp. 59–65.

[58] Durisi G., Koch T. & Popovski P. (2016) Toward massive, ultrareliable, and low-latency wireless communication with short packets. Proceedings of the IEEE 104, pp. 1711–1726.

[59] Azari A., Popovski P., Miao G. & Stefanovic C. (2017) Grant-free radio access for short-packet communications over 5G networks. In: GLOBECOM 2017-2017 IEEE Global Communications Conference, IEEE, pp. 1–7.

[60] Shahab M.B., Abbas R., Shirvanimoghaddam M. & Johnson S.J. (2020) Grant-free non-orthogonal multiple access for IoT: A survey. IEEE Communications Surveys & Tutorials .

[61] Dai L., Wang B., Ding Z., Wang Z., Chen S. & Hanzo L. (2018) A survey of non-orthogonal multiple access for 5G. IEEE communications surveys & tutorials 20, pp. 2294–2323.

[62] Sharma S.K. & Wang X. (2020) Toward massive machine type communications in ultra-dense cellular IoT networks: Current issues and machine learning-assisted solutions. IEEE Communications Surveys Tutorials 22, pp. 426–471.

[63] Ganti R.K. & Haenggi M. (2009) Spatial and temporal correlation of the interference in ALOHA ad hoc networks. IEEE Communications Letters 13, pp. 631–633.

[64] Mancuso V., Castagno P., Sereno M. & Marsan M.A. (2020) Modeling MTC and HTC radio access in a sliced 5G base station. IEEE Transactions on Network and Service Management .

[65] Andres-Maldonado P., Ameigeiras P., Prados-Garzon J., Navarro-Ortiz J. & Lopez-Soler J.M. (2017) Narrowband IoT data transmission procedures for massive machine-type communications. IEEE Network 31, pp. 8–15.

[66] Mekki K., Bajic E., Chaxel F. & Meyer F. (2018) Overview of cellular LPWAN technologies for IoT deployment: Sigfox, loRaWAN, and NB-IoT. In: International conference on pervasive computing and communications workshops, IEEE, pp. 197–202.

[67] Li Z., Chen J., Ni R., Chen S., Li X. & Zhao Q. (2017) Enabling heterogeneous mMTC by energy-efficient and connectivity-aware clustering and routing. In: Globecom Workshops, IEEE, pp. 1–6.

[68] Shaik Z.H., Björnson E. & Larsson E.G. (2020) Cell-free massive MIMO with radio stripes and sequential uplink processing. In: IEEE International Conference on Communications Workshops (ICC Workshops), pp. 1–6.

[69] Zhao J. (2019) A survey of intelligent reflecting surfaces (IRSs): Towards 6G wireless communication networks with massive MIMO 2.0.

[70] Wan Z., Gao Z., Renzo M.D. & Alouini M.S. (2020) Terahertz massive MIMO with holographic reconfigurable intelligent surfaces. ArXiv abs/2009.10963.

[71] Rajatheva N., Atzeni I., Bjornson E., Bourdoux A., Buzzi S., Doré J., Erkucuk S., Fuentes M., Guan K., Hu Y., Huang X., Hulkkonen J., Jornet J.M., Katz M., Nilsson R., Panayirci E., Rabie K.M., Rajapaksha N., Salehi M., Sarieddeen H., Svensson T., Tervo O., Tolli A., Wu Q. & Xu W. (2020) White paper on broadband connectivity in 6G. arXiv: Signal Processing .

[72] Hoseini S.A., Ding M. & Hassan M. (2017) Massive MIMO performance comparison of beamforming and multiplexing in the Terahertz band. In: Globecom Workshops, IEEE, pp. 1–6.

[73] Ahmadi A. & Semiari O. (2021) Reinforcement learning for optimized beam training in multi-hop Terahertz communications. ArXiv abs/2102.05269.

[74] Headland D., Monnai Y., Abbott D., Fumeaux C. & Withayachumnankul W. (2018) Tutorial: Terahertz beamforming, from concepts to realizations. Apl Photonics 3, p. 051101.

[75] Harter T., Füllner C., Kemal J., Ummethala S., Steinmann J., Brosi M., Hesler J., Bründermann E., Müller A.S., Freude W. et al. (2020) Generalized Kramers–Kronig receiver for coherent Terahertz communications. Nature Photonics 14, pp. 601–606.

[76] Chinnery D. & Keutzer K. (2007) Overview of the factors affecting the power consumption. In: Closing the Power Gap Between ASIC & Custom, Springer, pp. 11–53.

[77] Guo J., Durrani S., Zhou X. & Yanikomeroglu H. (2017) Massive machine type communication with data aggregation and resource scheduling. IEEE Transactions on Communications 65, pp. 4012–4026.

[78] Sim Y. & Cho D.H. (2020) Performance analysis of priority-based Access Class Barring scheme for massive MTC random access. IEEE Systems Journal 14, pp. 5245–5252.

[79] Bui A.T.H., Nguyen C.T., Thang T.C. & Pham A.T. (2019) A comprehensive distributed queue-based random access framework for mMTC in LTE/LTE-A networks with mixed-type traffic. IEEE Transactions on Vehicular Technology 68, pp. 12107–12120.

[80] Salam T., Rehman W.U. & Tao X. (2019) Data aggregation in massive machine type communication: Challenges and solutions. IEEE Access 7, pp. 41921–41946.

[81] Dawy Z., Saad W., Ghosh A., Andrews J.G. & Yaacoub E. (2016) Toward massive machine type cellular communications. IEEE Wireless Communications 24, pp. 120–128.

[82] Randhawa S. & Jain S. (2020) Cross-layer energy based clustering technique for heterogeneous wireless sensor networks. Wireless Personal Communications 114, pp. 1207–1233.

[83] Yuste-Delgado A.J., Cuevas-Martinez J.C. & Triviño-Cabrera A. (2020) A distributed clustering algorithm guided by the base station to extend the lifetime of wireless sensor networks. Sensors 20, p. 2312.

[84] Chatzikokolakis K., Kaloxylos A., Spapis P., Alonistioti N., Zhou C., Eichinger J. & Bulakci Ö. (2015) On the way to massive access in 5G: challenges and solutions for massive machine communications. In: International Conference on Cognitive Radio Oriented Wireless Networks, Springer, pp. 708–717.

[85] Jung W.S., Lim K.W., Ko Y.B. & Park S.J. (2011) Efficient clustering-based data aggregation techniques for wireless sensor networks. Wireless Networks 17, pp. 1387–1400.

[86] Bali R.S., Kumar N. & Rodrigues J.J. (2014) Clustering in vehicular ad hoc networks: taxonomy, challenges and solutions. Vehicular communications 1, pp. 134–152.

[87] Wang H. & Luo N. (2010) An improved ant-based algorithm for data aggregation in wireless sensor networks. In: International Conference on Communications and Mobile Computing, vol. 3, IEEE, vol. 3, pp. 239–243.

[88] Ali N., Faezeh Sadat B. & Zeynep O. (2012) A tree based data aggregation scheme for wireless sensor networks using GA. Wireless Sensor Network 2012.

[89] Atoui I., Makhoul A., Tawbe S., Couturier R. & Hijazi A. (2016) Tree-based data aggregation approach in periodic sensor networks using correlation matrix and polynomial regression. In: 2016 IEEE Intl Conference on Computational Science and Engineering (CSE) and IEEE Intl Conference on Embedded and Ubiquitous Computing (EUC) and 15th Intl Symposium on Distributed Computing and Applications for Business Engineering (DCABES), IEEE, pp. 716–723.

[90] Malak D., Dhillon H.S. & Andrews J.G. (2016) Optimizing data aggregation for uplink machine-to-machine communication networks. IEEE transactions on communications 64, pp. 1274–1290.

[91] Salam T., Rehman W.U. & Tao X. (2018) Cooperative data aggregation and dynamic resource allocation for massive machine type communication. IEEE Access 6, pp. 4145–4158.

[92] Hattab G. & Cabric D. (2017) Energy-efficient massive cellular IoT shared spectrum access via mobile data aggregators. In: 13th International Conference on Wireless and Mobile Computing, Networking and Communications, IEEE, pp. 1–6.

[93] Xu Y., Feng G., Liang L., Qin S. & Chen Z. (2017) MTC data aggregation for 5G network slicing. In: 23rd Asia-Pacific Conference on Communications, IEEE, pp. 1–6.

[94] Yang C., Li J., Guizani M., Anpalagan A. & Elkashlan M. (2016) Advanced spectrum sharing in 5G cognitive heterogeneous networks. IEEE Wireless Communications 23, pp. 94–101.

[95] Hu F., Chen B. & Zhu K. (2018) Full spectrum sharing in cognitive radio networks toward 5G: A survey. IEEE Access 6, pp. 15754–15776.

[96] Ahmad A., Ahmad S., Rehmani M.H. & Hassan N.U. (2015) A survey on radio resource allocation in cognitive radio sensor networks. IEEE Communications Surveys & Tutorials 17, pp. 888–917.

[97] Zhang L., Xiao M., Wu G., Alam M., Liang Y.C. & Li S. (2017) A survey of advanced techniques for spectrum sharing in 5G networks. IEEE Wireless Communications 24, pp. 44–51.

[98] Zhou K., Nikaein N., Knopp R. & Bonnet C. (2012) Contention based access for machine-type communications over LTE. In: 75th Spring Vehicular Technology Conference, IEEE, pp. 1–5.

[99] Chang C.H. & Hsieh H.Y. (2012) Not every bit counts: A resource allocation problem for data gathering in machine-to-machine communications. In: IEEE Global Communications Conference, pp. 5537–5543.

[100] Lioumpas A.S. & Alexiou A. (2011) Uplink scheduling for machine-to-machine communications in LTE-based cellular systems. In: IEEE GLOBECOM Workshops, pp. 353–357.

[101] López O.L.A., Alves H., Nardelli P.H.J. & Latva-aho M. (2018) Aggregation and resource scheduling in machine-type communication networks: A stochastic geometry approach. IEEE Transactions on Wireless Communications 17, pp. 4750–4765.

[102] López O.L.A., Alves H., Nardelli P.H. & Latva-aho M. (2019) Hybrid resource scheduling for aggregation in massive machine-type communication networks. Ad Hoc Networks 94, p. 101932.

[103] Huang Y.F., Tan T.H., Liu S.P., Liu T.Y. & Chen C.M. (2018) Performance of subcarrier allocation of D2D multicasting for wireless communication systems. In: Tenth International Conference on Advanced Computational Intelligence, IEEE, pp. 193–196.

[104] Kai Y., Wang J., Zhu H. & Wang J. (2018) Resource allocation and performance analysis of cellular-assisted OFDMA device-to-device communications. IEEE Transactions on Wireless Communications 18, pp. 416–431.

[105] Hou W., Li S., Sun Y., Zhou J., Yun X. & Lu N. (2019) Interference-aware subcarrier allocation for massive machine-type communication in 5G-enabled Internet of Things. Sensors 19, p. 4530.

[106] Wang Y., He Y., Xu C., Zhou Z., Mumtaz S., Rodriguez J. & Pervaiz H. (2019) Joint rate control and power allocation for low-latency reliable D2D-based relay network. EURASIP Journal on Wireless Communications and Networking 2019, pp. 1–14.

[107] Gupta P. & Kumar P.R. (2000) The capacity of wireless networks. IEEE Transactions on information theory 46, pp. 388–404.

[108] Coon J.P., Georgiou O. & Dettmann C.P. (2015) Connectivity scaling laws in wireless networks. IEEE Wireless Communications Letters 4, pp. 629–632.

[109] Mirmohseni M. & Papadimitratos P. (2014) Scaling laws for secrecy capacity in cooperative wireless networks. In: IEEE INFOCOM Conference on Computer Communications, pp. 1527–1535.

[110] Andrews J.G., Ganti R.K., Haenggi M., Jindal N. & Weber S. (2010) A primer on spatial modeling and analysis in wireless networks. IEEE Communications Magazine 48, pp. 156–163.

[111] Rajan M., Chandra M.G., Reddy L.C. & Hiremath P. (2008) Concepts of graph theory relevant to ad-hoc networks. Int. J. of Computers, Communications & Control 3, pp. 465–469.

[112] Kawahigashi H., Terashima Y., Miyauchi N. & Nakakawaji T. (2005) Modeling ad hoc sensor networks using random graph theory. In: Second Consumer Communications and Networking Conference, IEEE, pp. 104–109.

[113] ElSawy H., Hossain E. & Haenggi M. (2013) Stochastic geometry for modeling, analysis, and design of multi-tier and cognitive cellular wireless networks: A survey. IEEE Communications Surveys & Tutorials 15, pp. 996–1019.

[114] Haenggi M. (2012) Stochastic geometry for wireless networks. Cambridge University Press.

[115] Cox D.R. & Isham V. (1980) Point processes, vol. 12. CRC Press.

[116] Salehi M., Tabassum H. & Hossain E. (2018) Meta distribution of SIR in large-scale uplink and downlink NOMA networks. IEEE Transactions on Communications 67, pp. 3009–3025.

[117] Devroye L. (2006) Nonuniform random variate generation. Handbooks in operations research and management science 13, pp. 83–121.

[118] Asmussen S. & Glynn P.W. (2007) Stochastic simulation: algorithms and analysis, vol. 57. Springer Science & Business Media.

[119] Baccelli F. & Błaszczyszyn B. (2009), Stochastic geometry and wireless networks, volume I—theory, volume 3, no 3–4 of foundations and trends in networking.

[120] Dhillon H.S. & Chetlur V.V. (2020) Poisson Line Cox process: Foundations and applications to vehicular networks. Synthesis Lectures on Learning, Networks, and Algorithms 1, pp. 1–149.

[121] Choi C.S. & Baccelli F. (2018) Poisson Cox point processes for vehicular networks. IEEE Transactions on Vehicular Technology 67, pp. 10160–10165.

[122] Guo A. & Haenggi M. (2013) Spatial stochastic models and metrics for the structure of base stations in cellular networks. IEEE Transactions on Wireless Communications 12, pp. 5800–5812.

[123] Haenggi M. (2017) User point processes in cellular networks. IEEE Wireless Communications Letters 6, pp. 258–261.

[124] Yang J., Pan Z. & Guo L. (2020) Coverage and energy efficiency analysis for two-tier heterogeneous cellular networks based on Matérn hard-core process. Future Internet 12, p. 1.

[125] Lei T., Wen X., Lu Z., Jing W., Chen K. & Zhao X. (2016) A modified Matérn hard core point process for modeling and analysis of dense IEEE 802.11 networks. In: International Symposium on Wireless Communication Systems, pp. 608–612.

[126] Alfano G., Garetto M. & Leonardi E. (2011) New insights into the stochastic geometry analysis of dense CSMA networks. In: Proceedings IEEE INFOCOM, pp. 2642–2650.

[127] Haenggi M. (2011) Mean interference in hard-core wireless networks. IEEE Communications Letters 15, pp. 792–794.

[128] Li Y., Baccelli F., Dhillon H.S. & Andrews J.G. (2015) Statistical modeling and probabilistic analysis of cellular networks with Determinantal point processes. IEEE Transactions on Communications 63, pp. 3405–3422.

[129] Kong H.B., Wang P., Niyato D. & Cheng Y. (2017) Modeling and analysis of wireless sensor networks with/without energy harvesting using Ginibre point processes. IEEE Transactions on Wireless Communications 16, pp. 3700–3713.

[130] Ali A. & Vesilo R. (2017) Interference modelling in cellular networks with beta-Ginibre point process deployed base stations. In: IEEE 85th Spring Vehicular Technology Conference, pp. 1–6.

[131] Yazdanshenasan Z., Dhillon H.S., Afshang M. & Chong P.H. (2016) Poisson hole process: Theory and applications to wireless networks. IEEE Transactions on Wireless Communications 15, pp. 7531–7546.

[132] Lee C.h. & Haenggi M. (2012) Interference and outage in Poisson cognitive networks. IEEE Transactions on Wireless Communications 11, pp. 1392–1401.

[133] Deng N., Zhou W. & Haenggi M. (2014) A heterogeneous cellular network model with inter-tier dependence. In: IEEE Global Communications Conference, pp. 1522–1527.

[134] Afshang M. & Dhillon H.S. (2015) Spatial modeling of device-to-device networks: Poisson cluster process meets Poisson hole process. In: 49th Asilomar Conference on Signals, Systems and Computers, IEEE, pp. 317–321.

[135] Guo A., Zhong Y., Zhang W. & Haenggi M. (2016) The Gauss–Poisson process for wireless networks and the benefits of cooperation. IEEE Transactions on Communications 64, pp. 1916–1929.

[136] Liu L.y., Ma Z.g., Xue Y., Yan W.b. & Li Y.y. (2017) Research on coverage probability in ultra-dense 5G heterogeneous cellular networks based on Poisson clustered process. Wireless Personal Communications 95, pp. 2915–2930.

[137] Saha C., Afshang M. & Dhillon H.S. (2017) Poisson cluster process: Bridging the gap between PPP and 3GPP HetNet models. In: 2017 Information Theory and Applications Workshop (ITA), IEEE, pp. 1–9.

[138] Saha C., Dhillon H.S., Miyoshi N. & Andrews J.G. (2019) Unified analysis of HetNets using Poisson cluster processes under max-power association. IEEE Transactions on Wireless Communications 18, pp. 3797–3812.

[139] Afshang M., Saha C. & Dhillon H.S. (2016) Nearest-neighbor and contact distance distributions for Thomas cluster process. IEEE Wireless Communications Letters 6, pp. 130–133.

[140] Tang J., Chen G., Coon J.P. & Simmons D.E. (2017) Distance distributions for Matérn cluster processes with application to network performance analysis. In: IEEE International Conference on Communications, pp. 1–6.

[141] Wang Y. & Zhu Q. (2019) Performance analysis of clustered device-to-device networks using Mátern cluster process. Wireless Networks 25, pp. 4849–4858.

[142] Deng N. & Haenggi M. (2020) The energized point process as a model for wirelessly powered communication networks. IEEE Transactions on Green Communications and Networking 4, pp. 832–844.

[143] Baddeley A., Bárány I. & Schneider R. (2006) Stochastic Geometry: Lectures Given at the CIME Summer School Held in Martina Franca, Italy, September 13-18, 2004. Springer.

[144] Upton G., Fingleton B. et al. (1985) Spatial data analysis by example. Volume 1: Point pattern and quantitative data. John Wiley & Sons Ltd.

[145] Illian J., Penttinen A., Stoyan H. & Stoyan D. (2008) Statistical analysis and modelling of spatial point patterns, vol. 70. John Wiley & Sons.

[146] Haenggi M. & Ganti R.K. (2009) Interference in large wireless networks. Now Publishers Inc.

[147] Chiu S.N., Stoyan D., Kendall W.S. & Mecke J. (2013) Stochastic geometry and its applications. John Wiley & Sons.

[148] Li Y., Baccelli F., Dhillon H.S. & Andrews J.G. (2014) Fitting Determinantal point processes to macro base station deployments. In: IEEE Global Communications Conference, pp. 3641–3646.

[149] Deng N., Zhou W. & Haenggi M. (2014) The Ginibre point process as a model for wireless networks with repulsion. IEEE Transactions on Wireless Communications 14, pp. 107–121.

[150] Hirsch C., Moka S.B., Taimre T. & Kroese D.P. (2020) Rare events in random geometric graphs. preprint arXiv:2007.05965 .

[151] Yamada I. & Rogerson P.A. (2003) An empirical comparison of edge effect correction methods applied to k-function analysis. Geographical analysis 35, pp. 97–109.

[152] Protázio J.M.B., Pereira W.C., de F.E.J. & Castro (2010) Explicit formulas for an area based edge effect correction method and their application to Ripley's k-function.

[153] Farooq M.J., ElSawy H., Zhu Q. & Alouini M.S. (2017) Optimizing mission critical data dissemination in massive IoT networks. In: 15th International Symposium on Modeling and Optimization in Mobile, Ad Hoc, and Wireless Networks (WiOpt), IEEE, pp. 1–6.

[154] Gharbieh M., ElSawy H., Bader A. & Alouini M.S. (2017) Spatiotemporal stochastic modeling of IoT enabled cellular networks: Scalability and stability analysis. IEEE Transactions on Communications 65, pp. 3585–3600.

[155] Jiang N., Deng Y., Kang X. & Nallanathan A. (2018) Random access analysis for massive IoT networks under a new spatio-temporal model: A stochastic geometry approach. IEEE Transactions on Communications 66, pp. 5788–5803.

[156] Bader A., ElSawy H., Gharbieh M., Alouini M.S., Adinoyi A. & Alshaalan F. (2017) First mile challenges for large-scale IoT. IEEE Communications Magazine 55, pp. 138–144.

[157] Aftab N., Zaidi S.A.R. & McLernon D. (2020) Scalability analysis of multiple LoRa gateways using stochastic geometry. Internet of Things 9, p. 100132.

[158] Mahmood A., Sisinni E., Guntupalli L., Rondón R., Hassan S.A. & Gidlund M. (2018) Scalability analysis of a LoRa network under imperfect orthogonality. IEEE Transactions on Industrial Informatics 15, pp. 1425–1436.

[159] Azari A. & Cavdar C. (2018) Performance evaluation and optimization of LPWA IoT networks: A stochastic geometry approach. In: IEEE Global Communications Conference, pp. 206–212.

[160] Okegbile S.D., Maharaj B.T. & Alfa A.S. (2020) Stochastic geometry approach towards interference management and control in cognitive radio network: A survey. Computer Communications .

[161] Liu J., Wu G., Zhang X., Fang S. & Li S. (2020) Modeling, analysis, and optimization of grant-free NOMA in massive MTC via stochastic geometry. IEEE Internet of Things Journal .

[162] Hmamouche Y., Benjillali M. & Saoudi S. (2021) On the role of stochastic geometry in Sixth Generation wireless networks. In: 10th International Symposium on Signal, Image, Video and Communications.

[163] Baccelli F., Blaszczyszyn B. & Muhlethaler P. (2006) An ALOHA protocol for multihop mobile wireless networks. IEEE Transactions on Information Theory 52, pp. 421–436.

[164] Haenggi M. (2012) The local delay in Poisson networks. IEEE Transactions on Information Theory 59, pp. 1788–1802.

[165] Ibrahim H., Tabassum H. & Nguyen U.T. (2020) The meta distributions of the SIR/SNR and data rate in coexisting sub-6GHz and millimeter-wave cellular networks. IEEE Open Journal of the Communications Society 1, pp. 1213–1229.

[166] Haenggi M. (2015) The meta distribution of the SIR in Poisson bipolar and cellular networks. IEEE Transactions on Wireless Communications 15, pp. 2577–2589.

[167] Guruacharya S. & Hossain E. (2018) Approximation of meta distribution and its moments for Poisson cellular networks. IEEE Wireless Communications Letters 7, pp. 1074–1077.

[168] Baccelli F. & Błaszczyszyn B. (2010) A new phase transitions for local delays in MANETs. In: 2010 Proceedings INFOCOM, IEEE, pp. 1–9.

[169] Haenggi M. (2010) Local delay in static and highly mobile Poisson networks with ALOHA. In: IEEE International Conference on Communications, pp. 1–5.

[170] Wang Y., Haenggi M. & Tan Z. (2018) SIR meta distribution of k-tier downlink heterogeneous cellular networks with cell range expansion. IEEE Transactions on Communications 67, pp. 3069–3081.

[171] Salehi M., Mohammadi A. & Haenggi M. (2017) Analysis of D2D underlaid cellular networks: SIR meta distribution and mean local delay. IEEE Transactions on Communications 65, pp. 2904–2916.

[172] Zhong Y., Zhang W. & Haenggi M. (2014) Managing interference correlation through random medium access. IEEE Transactions on Wireless Communications 13, pp. 928–941.

[173] Kalamkar S.S. (2019) Reliability and local delay in wireless networks: Does bandwidth partitioning help? In: 2019 IEEE Global Communications Conference, pp. 1–6.

[174] Mnatsakanov R.M. (2008) Hausdorff moment problem: Reconstruction of probability density functions. Statistics & probability letters 78, pp. 1869–1877.

[175] Mnatsakanov R.M. & Hakobyan A.S. (2009) Recovery of distributions via moments. Lecture Notes-Monograph Series , pp. 252–265.

[176] Gil-Pelaez J. (1951) Note on the inversion theorem. Biometrika 38, pp. 481–482.

[177] Deng N. & Haenggi M. (2017) A fine-grained analysis of millimeter-wave device-to-device networks. IEEE Transactions on Communications 65, pp. 4940–4954.

[178] Deng N. & Haenggi M. (2018) The energy and rate meta distributions in wirelessly powered D2D networks. IEEE Journal on Selected Areas in Communications 37, pp. 269–282.

[179] Ibrahim H., Tabassum H. & Nguyen U.T. (2019) Meta distribution of SIR in dual-hop Internet-of-Things (IoT) networks. In: IEEE International Conference on Communications, pp. 1–7.

[180] Hayajneh A.M., Zaidi S.A.R., McLernon D.C., Win M.Z., Imran A. & Ghogho M. (2018) Optimal coverage and rate in downlink cellular networks: A SIR meta-distribution based approach. In: IEEE Global Communications Conference, pp. 1–7.

[181] Wang Y., Haenggi M. & Tan Z. (2017) The meta distribution of the SIR for cellular networks with power control. IEEE Transactions on Communications 66, pp. 1745–1757.

[182] Zhou S., Zhao J., Tan G. & Li X. (2019) A fine-grained analysis of wireless powered communication with Poisson cluster process. In: 11th International Conference on Wireless Communications and Signal Processing, IEEE, pp. 1–6.

[183] Kalamkar S.S. & Haenggi M. (2018) The spatial outage capacity of wireless networks. IEEE Transactions on Wireless Communications 17, pp. 3709–3722.

[184] Yu X., Cui Q., Wang Y., Li N., Tao X. & Valkama M. (2020) Stochastic geometry based analysis for heterogeneous networks: a perspective on meta distribution. Science in China Series F: Information Sciences 63, pp. 1–21.

[185] Haenggi M. (2018) Efficient calculation of meta distributions and the performance of user percentiles. IEEE Wireless Communications Letters 7, pp. 982–985.

[186] Mnatsakanov R. & Ruymgaart F. (2003) Some properties of moment-empirical CDFs with application to some inverse estimation problems. Mathematical Methods of Statistics 12, pp. 478–495.

[187] Abate J. & Whitt W. (1995) Numerical inversion of Laplace transforms of probability distributions. ORSA Journal on computing 7, pp. 36–43.

[188] Zhou X., Guo J., Durrani S. & Di Renzo M. (2017) Power beacon-assisted millimeter wave ad hoc networks. IEEE Transactions on Communications 66, pp. 830–844.

[189] Wang S. & Di Renzo M. (2019) On the meta distribution in spatially correlated non-Poisson cellular networks. EURASIP Journal on Wireless Communications and Networking , pp. 1–11.

[190] Kalamkar S.S. & Haenggi M. (2019) Simple approximations of the SIR meta distribution in general cellular networks. IEEE Transactions on Communications 67, pp. 4393–4406.

[191] Guo A. & Haenggi M. (2014) Asymptotic deployment gain: A simple approach to characterize the SINR distribution in general cellular networks. IEEE Transactions on Communications 63, pp. 962–976.

[192] Koufos K. & Dettmann C.P. (2019) The meta distribution of the SIR in linear motorway VANETs. IEEE Transactions on Communications 67, pp. 8696–8706.

[193] Di Renzo M., Wang S. & Xi X. (2018) Inhomogeneous double thinning—modeling and analysis of cellular networks by using inhomogeneous Poisson point processes. IEEE Transactions on Wireless Communications 17, pp. 5162–5182.

[194] López O.L., Alves H. & Latva-Aho M. (2019) Distributed rate control in downlink NOMA networks with reliability constraints. IEEE Transactions on Wireless Communications 18, pp. 5410–5423.

[195] El Sawy H. (2020) Rate adaptation and latency in heterogeneous IoT networks. IEEE Communications Letters .

[196] Kalamkar S.S. & Haenggi M. (2019) Per-link reliability and rate control: Two facets of the SIR meta distribution. IEEE Wireless Communications Letters 8, pp. 1244–1247.

[197] Kalamkar S.S. & Haenggi M. (2017) Distributed rate control for high reliability in Poisson bipolar networks. In: IEEE Global Communications Conference, pp. 1–6.

[198] Sun Y., Liu Q. & Wang H. (2020) SIR meta distribution in the heterogeneous and hybrid networks. Wireless Communications and Mobile Computing 2020.

[199] Deng N. & Haenggi M. (2018) The meta distribution of the SINR and rate in heterogeneous cellular networks. In: IEEE 29th Annual International Symposium on Personal, Indoor and Mobile Radio Communications, pp. 1–6.

[200] Luo Y., Shi Z. & Bu F. (2020) Analysis of SIR and rate meta distributions for 3D heterogenous ultra-dense networks with joint offloading and resource partitioning. IEEE Access 8, pp. 43067–43081.

[201] Yu X., Cui Q. & Haenggi M. (2019) SIR meta distribution for spatiotemporal cooperation in Poisson cellular networks. IEEE Access 7, pp. 73617–73626.

[202] Ali K., ElSawy H. & Alouini M.S. (2018) Meta distribution of downlink non-orthogonal multiple access (NOMA) in Poisson networks. IEEE Wireless Communications Letters 8, pp. 572–575.

[203] Mankar P.D. & Dhillon H.S. (2019) Meta distribution for downlink NOMA in cellular networks with 3GPP-inspired user ranking. In: IEEE Global Communications Conference, IEEE, pp. 1–6.

[204] Lei H., Gao R., Ren Z., Park K.H., Pan G. & Alouini M.S. (2021) The meta distributions of secrecy rate for the downlink NOMA systems. IEEE Wireless Communications Letters 10, pp. 291–295.

[205] Barros J. & Rodrigues M.R. (2006) Secrecy capacity of wireless channels. In: 2006 IEEE international symposium on information theory, IEEE, pp. 356–360.

[206] Liu Q. & Ball E.A. (2020) The meta distribution of the SIR for LoRaWANs with power control. IEEE Transactions on Industrial Informatics .

[207] Afzal A., Zaidi S.A.R., McLernon D., Ghogho M. & Feki A. (2017) M2M meets D2D: Harnessing D2D interfaces for the aggregation of M2M data. In: IEEE International Conference on Communications, pp. 1–6.

[208] Kim D.M., Sorensen R.B., Mahmood K., Osterbo O.N., Zanella A. & Popovski P. (2017) Data aggregation and packet bundling of uplink small packets for monitoring applications in LTE. IEEE Network 31, pp. 32–38.

[209] Saha C., Afshang M. & Dhillon H.S. (2017) 3GPP-inspired HetNet model using Poisson cluster process: Sum-product functionals and downlink coverage. IEEE Transactions on Communications 66, pp. 2219–2234.

[210] Afshang M., Saha C. & Dhillon H.S. (2017) Nearest-neighbor and contact distance distributions for Matérn cluster process. IEEE Communications Letters 21, pp. 2686–2689.

[211] Lu X., Salehi M., Haenggi M., Hossain E. & Jiang H. (2021) Stochastic geometry analysis of spatial-temporal performance in wireless networks: A tutorial. CoRR abs/2102.00588. URL: `https://arxiv.org/abs/2102.00588`.

[212] Herath P., Tellambura C. & Krzymien W.A. (2015) Stochastic geometry modeling of cellular uplink power control under composite Rayleigh-lognormal fading. In: IEEE 82nd vehicular technology conference, pp. 1–5.

[213] López O.L.A., Alves H. & Latva-Aho M. (2018) Rate control under finite blocklength for downlink cellular networks with reliability constraints. In: 15th International Symposium on Wireless Communication Systems, IEEE, pp. 1–6.

[214] Yu X., Li C., Zhang J. & Letaief K.B. (2019) Stochastic Geometry Analysis of Multi-Antenna Wireless Networks. Springer.

[215] Thompson I. (2011), NIST handbook of mathematical functions, edited by Frank WJ Olver, Daniel W. Lozier, Ronald F. Boisvert, Charles W. Clark.

[216] Anderssen R.S., Husain S.A. & Loy R. (2003) The Kohlrausch function: properties and applications. Anziam journal 45, pp. C800–C816.

[217] Ammar H.A., Nasser Y. & Artail H. (2018) Closed form expressions for the probability density function of the interference power in PPP networks. In: IEEE International Conference on Communications, pp. 1–6.

[218] Ali M.M. & Woo J. (2005) Inference on reliability p (y< x) in the Levy distribution. Mathematical and computer modelling 41, pp. 965–971.

[219] O'Reilly F. & Rueda R. (1998) A note on the fit for the Levy distribution. Communications in Statistics-Theory and Methods 27, pp. 1811–1821.

[220] Clavier L., Pedersen T., Rodríguez I., Lauridsen M. & Egan M. (2020) Experimental evidence for heavy tailed interference in the IoT. IEEE Communications Letters , pp. 1–5.